Understanding the biodegradation of PHBV/Cellulose composites in mesophilic anaerobic digestion

Paul Derkenne, Lucile Chatellard, Fabrice Beline, Anne-Catherine Pierson-Wickmann, Nathalie Gontard, P. Dabert

Science of the Total Environment 959 (2025) 178224

Contents lists available at ScienceDirect

Science of the Total Environment

journal homepage: www.elsevier.com/locate/scitotenv

Understanding the biodegradation of PHBV/Cellulose composites in mesophilic anaerobic digestion

Paul Derkenne [a,b,*], Lucile Chatellard [b], Fabrice Béline [a], Anne-Catherine Pierson-Wickmann [c], Nathalie Gontard [d], Patrick Dabert [a]

[a] UR 1466 OPAALE, INRAE, 17 avenue de Cucillé, F-35044 Rennes, France
[b] UMR IATE, Université de Montpellier, 163 rue Auguste Broussonnet, F-34090 Montpellier, France
[c] UMR Géosciences, Université de Rennes, F-35000 Rennes, France
[d] UMR IATE, INRAE, 2 place Pierre Viala, F-34060 Montpellier, France

HIGHLIGHTS

- PHBV materials show high degradation in mesophilic anaerobic digestion in 60 days.
- PHBV/Cellulose composites with higher cellulose content degrade faster.
- Material analysis reveals surface degradation mechanism.
- Biofilm attached to the materials is enriched in *Clostridium* and *Ruminofilibacter*.

GRAPHICAL ABSTRACT

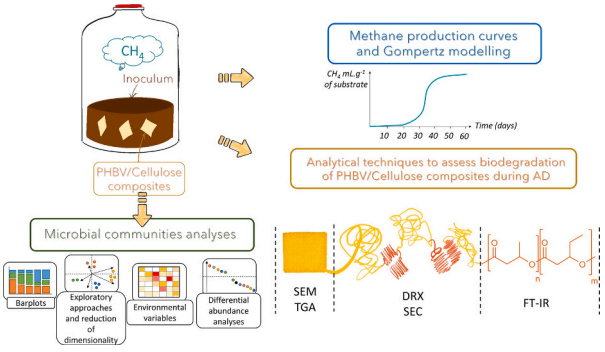

ARTICLE INFO

Editor: Elena Paoletti

Keywords:
Biodegradable plastics
Anaerobic digestion
Plastic degradation
Microplastics
Biowaste

ABSTRACT

Biodegradable plastics have been developed as alternative materials to prevent the environmental damage of conventional plastics on ecosystems. However, their end of life depends on environmental conditions in which they are disposed of. Their management in anaerobic digestion (AD) remains a topic of debate and needs further investigation. This study assesses the behaviour of PHBV, a prominent bio-based biodegradable plastic, blended with cellulose fibres in mesophilic AD conditions. Results show that degradation depends on material characteristics such as its specific surface area and cellulose content. Nearly complete biodegradation is observed for 1 mm diameter powder and 67 % degradation for 2 × 2 cm films over 57 days of AD at 38 °C. Biodegradation is faster with higher cellulose content up to 40 %. Morphological, structural, and functional analyses indicate that biodegradation occurs primarily through surface erosion, resulting in reduced polymers molecular weight and crystallinity, along with shifts in functional ester groups. Specific microbial genera, such as *Ruminofilibacter*, *Thiospeudomonas*, and *HN.HF0106*, were abundant in the planktonic phase, while *Ruminofilibacter*, *Clostridium*

Abbreviations: AD, anaerobic digestion; BMP, Biochemical Methane Potential; DSC, differential scanning calorimetry; Mw, weight average molar mass; OTU, Operational Taxonomic Unit; PHBV, poly(hydroxybutyrate-co-hydroxyvalerate); SEM, scanning electron microscopy; TGA, thermogravimetric analyses; VFAs, volatile fatty acids.

* Corresponding author at: UR 1466 OPAALE, INRAE, 17 avenue de Cucillé, F-35044 Rennes, France.
E-mail address: paul.derkenne@inrae.fr (P. Derkenne).

https://doi.org/10.1016/j.scitotenv.2024.178224
Received 5 September 2024; Received in revised form 19 December 2024; Accepted 19 December 2024
Available online 27 December 2024

sensu stricto *7*, *UCG.012*, and *Treponema* dominated the biofilm during AD. This research aims to provide deeper understanding of PHBV degradation mechanisms in AD, crucial for effective management in such conditions.

1. Introduction

The accumulation of conventional plastic waste in the biosphere is a potential threat for the ecosystems health (Lee et al., 2023). Biodegradable plastics, whose persistence in the environment is shorter than conventional ones, have been produced to tackle this concern (Moshood et al., 2022). They could replace petroleum-based plastics in the packaging sector which currently count for 40 % of the global plastic production (Jabeen et al., 2015). More specifically, conventional food packaging used for fresh products such as meat, fish or cheese are used only once, for less than one year, and cannot be recycled because of food contamination (Geyer et al., 2017; Dedieu et al., 2023). The production of biodegradable films and trays for fresh food packaging would enable their disposal alongside biowaste in recovery processes such as composting and anaerobic digestion (García-Depraect et al., 2022a). This would help closing the cycle of carbon in a bioeconomy loop and reduce the global impact of agri-food industry on the environment.

Anaerobic digestion (AD) is a well-known technology to valorise organic residues in biogas and digestate which can be used respectively as green energy and fertiliser (Song et al., 2021). However, food packaging plastics are often found in biowaste streams raising concerns about the becoming of those materials in AD plants. Recent reviews underlined the presence of microplastics (<5 mm) in biowaste, compost and digestate, mostly resulting from the fragmentation of conventional food packaging during biowaste treatment (Porterfield et al., 2023; Sholokhova et al., 2022). The use of compost and digestate as organic fertilizers increases the amount of plastic particles found in agricultural soils (Colombini et al., 2022; Kedzierski et al., 2023).

Among all biodegradable polymers currently produced, poly(3-hydroxybutyrate-*co*-3-hydroxyvalerate (PHBV) is especially interesting for food packaging (Acharjee et al., 2023). It is authorized for food contact applications by the European Plastics Regulation (EU) No 10/2011. Its mechanical properties make it suitable for industrial processing (Bonnenfant et al., 2023; Dedieu et al., 2023). However, it is commonly produced by pure bacterial culture fed with pure substrate such as glucose or starch, making its production more expensive than other conventional or biodegradable polymers (McAdam et al., 2020). To reduce the final cost of PHBV-based materials, other polymers such as cellulose can be added as fillers in the polymer matrix, forming a cheaper blended material (Conceição et al., 2023). Adding cellulose in the polymer matrix makes the resulting material more flexible (Sánchez-Safont et al., 2019) and prone to biodegradation especially under AD (Iwańczuk et al., 2015; Vu et al., 2022). However, the biological conversion of PHBV and of its cellulose composites is still poorly understood, it is relevant to study their behaviour in AD to validate their complete degradation.

Plastic degradation in the environment is a complex process that depends on both the material properties and a combination of abiotic and biotic environmental factors (Bher et al., 2022; Lucas et al., 2008; Zhang et al., 2021). The process is often described as having three to four steps: deterioration, fragmentation, assimilation, and mineralization. Deterioration, also known as aging or weathering, is the first step and involves alteration of the colour, the mechanical properties, and the bulk structure of the material due to abiotic factors e.g. light, thermal and chemical degradation, or mechanical stresses. Fragmentation, or disintegration, is the second step and results in the material breaking down into smaller pieces due to both chemical and enzymatic scission of plastic polymers. The last steps of plastic degradation involve the internalization of oligomers into the cells of microorganisms and their subsequent mineralization into CO_2 and H_2O under aerobic conditions, or into methane (CH_4), CO_2, organic acids and H_2O under anaerobic conditions. Finally, according to Meereboer et al. (2020a) and Bher et al. (2022), plastics seem to degrade by surface and bulk erosion, with the former involving enzymatic degradation at the surface of the material and the latter involving small chemical and free radical molecules penetrating the material and promoting both bulk and surface degradation.

Several methods have been developed to follow the biodegradation of plastics under AD conditions (Ruggero et al., 2019; Cazaudehore et al., 2022). The most used is the biochemical potential test (BMP), which consists of measuring methane production during batch incubations of an anaerobic inoculum with the material to be tested as the sole carbon source (Ribeiro et al., 2020). In such BMP tests, PHBV powder exhibited 83 % to 96 % biodegradation within 20 to 35 days at 35 °C to 37 °C in AD conditions (Budwill et al., 1992; Reischwitz et al., 1997; Ryan et al., 2017a). However, this test does not provide any information on the evolution of the material structure during degradation. To do so, thermal, physical and chemical analyses must be performed (Baidurah, 2022). For PHBV, such investigations have been done in soil (Lyshtva et al., 2024), in aging conditions (Antunes et al., 2020; Deroiné et al., 2014) and in marine environnements (Meereboer et al., 2020a). They demonstrated an alteration of the PHBV material morphological properties, a material mass loss, and shifts in the chemical bonds and crystallinity structure of the polymer. However, to our knowledge, no such investigation has been done to analyse the degradation of PHBV or PHBV/Cellulose composites under anaerobic digestion conditions.

The aim of this study is to improve the understanding of the degradation mechanisms of PHBV and of its cellulose composites under mesophilic AD by using a global approach combining: (i) measuring the methane production kinetics, (ii) analysing the changes in material properties, (iii) monitoring the microbial community dynamics, and (iv) in deep statistical analysis of these different parameters.

2. Materials and methods

2.1. Production of PHBV and PHBV/Cellulose biodegradable plastics

The poly(3-hydroxybutyrate-*co*-3-hydroxyvalerate (PHBV) pellets with 3 % of 3-hydroxyvalerate were supplied by Tianan® (grade PHI 003 — China). Pure cellulose particles under the commercial name of Arbocel® B00 were used as fillers to produce PHBV/Cellulose composites. Several percentages of cellulose content were targeted: 0 %, 10 %, 20 % 30 % and 40 % in mass. The PHBV was initially extruded with 0.05 % in weight of boron nitride (Sigma Aldrich reference 255475) used as nucleating agent, in order to facilitate its crystallization. All materials underwent an additional extrusion without or with cellulose (0 to 40 %) to produce PHBV/Cellulose blended materials The obtained pellet materials were shaped into films (300 μm thickness, 12 × 12 cm) using a heated hydraulic press (20 T, Pinette Emidecau Industries, Chalon-sur-Saône) heating at 180 °C during 9 min in a square aluminium mould. The properties of the PHBV and PHBV/Cellulose composites are presented in the supplementary material (Table S1). It must be noticed that increasing the amount of cellulose into the PHBV polymer to >40 % did not allow the production of cohesive films.

For the production of microplastics, one part of the thermopressed films previously shaped were milled using an impact mill (IKA A10) operating at 25,000 rpm, and sieved to collect particles of about 1 mm by using a mechanical sieving machine (ROTEX, 1 mm) — namely *powders*. The particle size distribution of the resulting powder was evaluated thanks to laser granulometry (Malvern Mastersizer 2000 Instrument Ltd., United Kingdom) (results gathered in Table S2). The second part of films was cut into pieces of 1 × 1 cm and 2 × 2 cm —

namely *films*.

2.2. Measure of plastics biodegradation through Biochemical Methane Potential (BMP) tests

2.2.1. BMP set-up

The inoculum used was a digestate taken from an experimental 10 m^3 pilot-scale platform (Valdimeta Saint-Gilles, France) fed with pig manure and operating at 38 °C. Before any experiment, the inoculum was depleted for 7 days at 38 °C to consume the residual fermentable organic matter, until the biogas production was minimal. Its dry matter content (DM) was measured by drying the sample at 105 °C for 48 h, and its volatile solid (VS) content by loss-on-ignition at 550 °C for 5 h. This VS content, assimilated to the microorganisms able to degrade the substrates, was used to calculate the mass of inoculum and substrate (cellulose, PHBV, or PHBV/Cellulose composite) to introduce in the BMP tests ensuring an inoculum-to-substrate ratio (ISR) equals to 1 as described by Jin et al. (2022). The initial pH of the digestate was of 8.6 and it was measured at the end of each experiment to assess potential acidification of the medium.

The BMP tests were performed using 572 mL batch bottles filled with 40 g of inoculum, about 1 g of substrate under the form of powder or films, and 95 mL of tap water to reach a headspace volume of 435 mL. The organic loading of the test was 24.4 g VS·L^{-1}. All substrates were tested in triplicate. Degradation of the Arbocel® B00 cellulose was used as a positive control. Three bottles only containing the inoculum were used to measure the biogas produced by the consumption of the inoculum residual organic matter (i.e. endogenous methane production). The BMP bottles were flushed with nitrogen before being incubated at 38 °C without agitation. Manual mixing was performed every two days, before gas pressure measurement, done with a manometer (2023P, Digital Instrumentation Ltd., Worthing, United Kingdom). When the pressure inside the bottle exceeded 1300 mbar, the gas was sampled with a 25 mL gas-tight syringe and stored in a hermetic vial for gas content analysis within 2 weeks.

2.2.2. Experimental strategy and sampling

The maximum biodegradation potential was measured for each material in the form of powder and 1 × 1 cm square pieces. Methane production was monitored until the stationary phase, attesting the end of the material biodegradation process, i.e. after 57–60 days of incubation.

Physico-chemical change of the material and microbial communities involved in the biodegradation were analysed during the time by sacrificing three reactors at 10, 20, 30, 40 and 50 days of digestion. The materials were cut into 2 × 2 cm pieces for this specific observation in order to get enough material during the biodegradation process. The plastic films and residues were recovered from the liquid medium by sieving at 500 μm and 100 μm. A part of the films was gently washed with sterile distilled water to remove microorganisms unattached to their surface, and stored at −20 °C for analysis of the attached microbial community. The other part of the films was strongly washed with sterile distilled water to remove a maximum of attached microorganisms, and dried in vacuum oven for 3 days before performing material analyses. Finally, about 40 mL of the BMP liquid medium was centrifuged for 10 min at 10,000*g*. The supernatant was stored at −20 °C before volatile fatty acids (VFAs) and Chemical Oxygen Demand (COD) analyses. The pellet was also stored at −20 °C for microbial community and solid COD analyses. Finally, a BMP bottle filled only with films and tap water was incubated at 38 °C under anaerobic conditions to analyse the impact of abiotic factors on material properties.

2.2.3. Chemical analyses

The proportion of CH_4 and CO_2 in biogas were determined by gas chromatography (GC) (Agilent 6890N) with FID flame ionisation detector equipped with a hydrogen generator (Domnick Hunter), a pre-column (Porapak N 0. 9N) and a packed column (Porapak Q 4M). Injector, oven and detector temperatures were respectively of 100 °C, 70 °C and 300 °C. The carrier gas was N_2 at a flow rate of 44 mL min^{-1}.

The concentrations of AD intermediate metabolites in the BMP tests, namely acetic, propionic, butyric, isobutyric and valeric volatile fatty acids (VFAs), were determined using a GC–MS (Agilent 7693A Automatic Liquid Sampler) as follow. Briefly, each sample is injected in the GC–MS system and heated in an oven at 250 °C for 40 min to ensure proper volatilization. The samples are then transferred into the column for separation, and molecules are detected and quantified by the mass detector. A calibration curve was established for each VFA to determine their concentration in each sample. Five concentrations were chosen for the calibration: 0.25, 0.5, 1, 2 and 5 g·L^{-1}.

The COD of all substrates were measured in triplicate using a METROHM® automatic titration device and a bench digestion Behrotest TRS 200. Chromium (VI) salts and sulphuric acid were used as oxidizing agents followed by a back titration performed with Mohr's salt. Copper phthalocyanine was used as control.

2.2.4. Material biodegradation estimation

The substrate biodegradation was estimated by two approaches:

First, it was calculated from the BMP biogas production as detailed in Jin et al. (2022). The endogenous methane production measured on BMP without substrate was subtracted from the methane produced in presence of substrate alone, to obtain the substrate conversion into methane. Then the material biodegradation was calculated by dividing this experimental methane production by the theoretical methane production as presented in Eq. 1:

$$\%\text{Biodegradation} = \frac{\text{Experimental methane production}}{\text{Theoretical methane production}} \times 100 \quad (1)$$

The theoretical methane production was estimated by the Buswell equation (Eq. 2) with a substrate defined as $C_xH_yO_z$:

$$\text{Theoretical methane production } (\text{mL } CH_4 \bullet g^{-1}\text{of substrate}) = \frac{22.4 \times \left(\frac{x}{2} + \frac{y}{8} - \frac{z}{4}\right)}{(12x + y + 16z)} \quad (2)$$

Second, ultimate degradation can also be estimated using experimental COD values (Eq. 3):

$$\%\text{Biodegradation} = \frac{\text{Experimental methane production}}{\text{COD of substrate}} \times \text{COD(methane)} \times 100 \quad (3)$$

With COD (methane) equals to 398 mL CH_4·g^{-1} at 38 °C (Zhang, 2014).

2.2.5. Modelling and statistical analysis

Cumulative methane production was modelled for each condition using a modified Gompertz model (García-Depraect et al., 2022a; Lebon et al., 2019; Ryan et al., 2017b) as presented in Eq. 4.

$$Y(t) = Y_0 \times exp\left[- exp\left(\frac{Y_{max} \times exp(1)}{Y_0} \times (\lambda - t) + 1 \right) \right] \quad (4)$$

where:

- $Y(t)$ is the cumulative methane production at time t in mL CH_4·gVS^{-1}
- Y_0 is the ultimate methane produced in mL CH_4·g VS^{-1}
- λ is the lag time in days
- Y_{max} is the maximal methane production rate in mL CH_4·g VS^{-1}·d^{-1}

Y_0, Y_{max}, and λ were determined with R software using the Nonlinear Least Squares method using nlsm function of the minpack.lm package (Cazaudehore et al., 2022). Statistical analysis were conducted on parameters across samples using ANOVA and Tukey HSD tests to assess the

significant differences between the reactors. The model reliability was evaluated by calculating the root-mean-square error (RMSE) and the homoscedasticity and normality of residuals from the model (Ware and Power, 2017).

2.3. Monitoring of plastic degradation

2.3.1. Attenuated total reflectance Fourier transform infrared spectroscopy (ATR-FTIR)

Attenuated total reflectance Fourier transform infrared spectroscopy (ATR-FTIR) was used to assess chemical bonds of materials during the biodegradation process. The ATR-FTIR spectra were registered with a spectrometer PerkinElmer (Spectrum 1000, spectrum for windows software) equipped with a ZnSe crystal with an incidence angle of 45° and 12 reflections. The background spectra were recorded in the air. 124 scans were taken per spectrum using a resolution of 2 cm^{-1} (Habibi et al., 2022). The analysed data spectra were baseline corrected using the software Fytik® and normalized to the peak associated with the C—H group of 1456 cm^{-1} which is known to be a chemical linkage independent to the degradation of PHBV (Abbasi et al., 2022).

2.3.2. Size Exclusion Chromatography (SEC)

Size Exclusion Chromatography (SEC) analyse, allowing the determination of the polymers average molar mass in number (M_n) and in mass (M_w) as well as dispersity, was performed at the Technopolym laboratory (Toulouse, France). The samples were dissolved in chloroform at concentrations between 3 and 5 mg/mL in closed tubes. They were then heated to reflux at 70 °C with stirring in an oil bath for at least 2 h to reach complete dissolution of materials. All samples were filtered through 0.45 μm before being analysed in SEC using Polytetrafluoroethylene membrane filter) and 2 Agilent PL gel columns (5 μm Mixed C). Products at the end of the columns were detected using: a differential refractometer detector (Optilab Rex Wyatt, $T = 35$ °C), a three-angles static light scattering detector (TREOS Wyatt, laser = 658 nm) and a UV detector (Shimadzu SPD-M20A, = 254 nm). It should be noticed the cellulose remains in the aqueous phase after dissolution of materials due to its poor solubility in chloroform and it is not analysed in this technique.

2.3.3. Wide-angle X-ray scattering (WAXS) and small-angle X-ray scattering (SAXS)

Polymer crystallinity was measured by X-ray diffraction with an in-house setup at Charles Coulomb laboratory (University of Montpellier, France). Briefly, a high brightness low power X-ray tube, coupled with aspheric multilayer optic (GeniX3D from Xenocs), delivers an ultralow divergent beam (0.5 mrad, $\lambda = 0.15418$ nm). Scatterless slits are used to give a clean 0.7 mm beam diameter with a flux of 35 Mphotons/s at the sample. Measurements are performed in a transmission configuration and scattered intensity is measured by a 2D "Pilatus" 300 K pixel detector by Dectris (490 * 600 pixels) with pixel size of 172 × 172 μm^2, at a distance from the sample of 0.2 m and 1.9 m for respectively WAXS and SAXS configurations. An empty cell is used to rectify all sample intensity values.

The crystallinity degree (X_c) is evaluated from the WAXS spectra by measuring the ratio between the crystalline areas and the total area of diffraction peaks. The area of the diffraction profile is assessed by peaks deconvolution using the Fityk® software with PseudoVoigt peak mode. PHBV crystallization occurs according to an orthorhombic crystalline structure which Miller's equation can be written as follow (Eq. 5):

$$d_{hkl} = \frac{1}{\sqrt{\frac{h^2}{a^2} + \frac{k^2}{b^2} + \frac{l^2}{c^2}}} \quad (5)$$

With d_{hkl} the d-spacing between adjacent planes, (*hkl*) the Miller indexes and a, b, c the lattice parameters for an orthorhombic crystalline structure, the d-spacing was determined from the Bragg's law with n the order of reflection:

$$n\lambda = 2d_{hkl} sin(\theta_{nhnknl})$$

The lattice parameters (a, b, c) were calculated from diffraction peaks (020), (110), (121) at respectively 13.5°, 16.8°, and 25.2° (2θ). Finally, the crystal size (L in nm) was evaluated using the Sherrer equation at the most intense crystalline diffraction peak at 13.5° (020): $L = K \cdot \lambda / (\beta - \beta_0) \cdot \cos(\theta)$. K is the Sherrer constant (0.9) and β is the peak width of half intensity (rad) corrected by $\beta_0 = 0.0026$ rad for instrumental line broadening.

2.3.4. Scanning electron microscopy (SEM)

SEM was used to visualize the surface of non-degraded and degraded materials. It was performed using a JSM 7100F (JEOL) microscope at the ScanMat laboratory (University of Rennes, France). The microscope is operating at a 6 mm working distance, with an accelerating voltage of 20 kV. Samples were prepared with gold metallization on carbon tape. SEM pictures were captured at four different magnifications (150×, 500×, 1000×, and 2500×) for each material, except for PHBV/Cellulose 80/20 and 60/40 where only 150× and 500× magnifications were possible (material degradation was too important at higher magnifications).

2.3.5. Thermogravimetric analyses

Thermogravimetric analysis (TGA) measures weight changes in a material as a function of increasing temperature under a controlled atmosphere of nitrogen or air. It allows monitoring the evolution of thermal stability and material composition. Analyses were performed with a Mettler TGA2 apparatus (Schwerzebbach, Switzerland) equipped with a Xp5U balance (precision of 0.0001 mg). Each analysis was carried out using 150 μL aluminium oxide crucibles (ME 24-124, Germany) filled with approximately 10 mg of material subjected to a 50 mL·min^{-1} nitrogen flow. All samples were heated from 25 °C to 900 °C with a heating rate of 10 °C·min^{-1}. Analyses were performed in duplicate. The degradation temperature of each material component as well as the composite composition during biodegradation were evaluated using the first derivate of the mass loss curve as described by Ruggero et al. (2019).

2.3.6. Differential scanning calorimetry (DSC)

The thermomechanical properties of the materials were determined by differential scanning calorimetry (DSC). DSC measures the amount of heat required to raise the temperature of a material relative to a reference, as a function of the applied temperature. The resulting thermogram enables measuring the glass transition temperature, the melting and crystallization temperatures and the crystallinity of the material. Analysis were carried out using a Q20 modulated DSC from TA instruments (New Castle, USA). Tzero Aluminium pans (TA Instruments New Castle, USA) were filled with about 10 mg of sample and hermetically sealed. The sealed pans were then subjected to 50 mL·min^{-1} nitrogen gas flow during the analysis. DSC analysis is divided in four thermal ramps: samples are first cooled down to −40 °C at a cooling rate of 10 °C·min^{-1}. They are then heated to 200 °C before being cooled down back to −40 °C and heated again to 200 °C at the rate of 10 °C·min^{-1}. The first heating erases any thermal history in material. Crystallization enthalpies are evaluated by integrating peaks on thermograms using the TA Analysis Software. Degree of crystallinity (X_c) was measured using the melting enthalpy with the following Eq. (6):

$$X_c = \frac{\Delta H_c}{\Delta H^{\circ}(PHBV)} \quad (6)$$

where $\Delta H^{\circ}(PHBV)$ corresponds to the melting enthalpy of the 100 % crystalline PHBV, i.e. 109 J·g^{-1} (Dedieu et al., 2023). Triplicates were performed in order to obtain the most precise and reproducible measures.

2.4. Microbial community analyses

2.4.1. DNA extractions and 16S rDNA sequencing

DNA extractions were realised using the Macherey–Nagel NucleoSpin® Soil kit according to manufacturer's instructions. DNA of the BMP tests' planktonic microbial communities was extracted from 250 mg of frozen pellets of BMP liquid medium collected as described in Section 2.2.2. DNA of the microbial populations attached to the materials was obtained by doing DNA extraction directly on one piece of plastic material stored at −20 °C (about 1 cm^2). Mechanical lysis used a FastPrep-24 instrument with 2 times 30 s shaking at 5 $m{\cdot}s^{-1}$ in SL1 lysis buffer with SX enhancer. Samples were cooled down on ice for 30 s between the two shaking steps. DNA were eluted in 50 μL of elution buffer. The amount and quality of the recovered DNA was estimated using spectrophotometry with an Eppendorf BioPhotometer® D30 and by 1 % agarose gel electrophoresis in TBE 1×. Control DNA extractions were performed on pristine plastic materials to detect potential contaminations.

Bacterial and archaeal communities were determined by Illumina MiSeq sequencing of the 16S rRNA gene V4–V5 variable regions using universal PCR primers 515F (5′-GTGYCAGCMGCCGCGGTA-3′) (Cardona et al., 2022) and 928R (3′-CCCCGYCAATTCMTTTRAGT-5′) (Wang and Qian, 2009), with Illumina overhang adapters. Libraries preparation and sequencing were performed by the INRAE PROSE Research Unit (Antony, France) according to the 16S Metagenomic Sequencing Library Preparation protocol from Illumina as described in the supplementary material.

2.4.2. Bioinformatics and data processing

The Illumina sequencing raw data were transformed on the Galaxy FROGS pipeline of the French National Research Institute for Agriculture, Food, and the Environment Galaxy portal (INRAE Jouy-en-Josas, France) (Escudié et al., 2018). Sequences were merged, denoised and dereplicated using the pre-processing tools of the system. Clustering was made by swarm with an aggregation distance of one. Minor ASVs, consisting of <0.0005 % of the total sequences, and chimera ASVs were withdrawn. Finally, the taxonomic assignment of the ASVs was performed by BLAST (NCBI, http://www. ncbi.nlm.nih.gov/BLAST) using the 16S SILVA Pintail 100 138.1 reference database.

Statistical analyses were carried out on Rstudio (version 4.3.3). The package phyloseq was used to manipulate more easily the raw data from the BIOM file to normalize samples. The rarefaction of sequences was performed using the *rarefy_even_depth()* function on the minimal number of sequences (3959). Bar plots of the relative abundance were obtained using *fantaxtic* package. Ward clustering trees were built using *hclust()* function from *vegan* package. The function *env.fit()* from *vegan* is used to select the more correlated variables to the ordination axes. The Spearman correlation matrix was plotted using the *corrplot* package to select ASVs correlated with environmental variables. *BestNormalize()* was used to transform raw environmental variables data before performing the correlation matrix. The *DESeq2* package was used for differential abundant analysis.

3. Results and discussions

3.1. Increasing the amount of cellulose in PHBV matrices speeds up their degradation

Fig. 1 shows the cumulative methane production obtained from the BMP tests of all materials, e.g. PHBV alone and PHBV/Cellulose blended at 90/10, 80/20, 70/30, and 60/40, in powder or 1 × 1 cm film form. The endogenous ultimate methane production accounts for approximately 13 % of the PHBV/Cellulose composites methane production, which is much lower than substrate methane production itself. This supports the relevant choices of ISR of 1/1 and inoculum used. High standard deviation values are observed during the exponential phase resulting from slightly delayed biogas production from one bottle to another within the triplicates. The kinetic parameters of methane production were estimated for all replicates by the modified Gompertz equation, and resume in supplementary Table S3.

As powder (Fig. 1a), all materials reached a similar ultimate methane production of 651 ± 87 to 727 ± 38 mL $CH_4{\cdot}g\ VS^{-1}$ within 40–57 days (Kruskal-Wallis test with $p_{value} = 0.83$). These values are similar to the 630 mL $CH_4{\cdot}g\ VS^{-1}$ depicted by Ryan et al. (2017a) in 56 days of AD at 37 °C. Increasing the proportion of cellulose from 0 to 40 % in the PHBV/Cellulose composites resulted to a faster biodegradation process by reducing the lag phase up to 43 %, e.g. from 23 to 13 days. The effect seems stronger for composites having >20 % cellulose (Fig. 1a). The cellulose content did not significantly change the maximal methane production rate that remained between 48 ± 34 and 62 ± 10 mL $CH_4{\cdot}day^{-1}{\cdot}g\ VS^{-1}$ (Kruskal-Wallis test with $p_{value} = 0.74$, Fig. S1a). The percentages of biodegradation range from 96 % to 117 %, calculated from the Buswell equation. Values higher than 100 % can be explained by measurements and/or calculation uncertainties, but suggest a complete degradation of the material powders.

Previous works also reflect that the addition of natural fibres such as cellulose into polymeric matrices accelerate the biodegradability of the composite material by shortening the lag phase (Gómez and Michel,

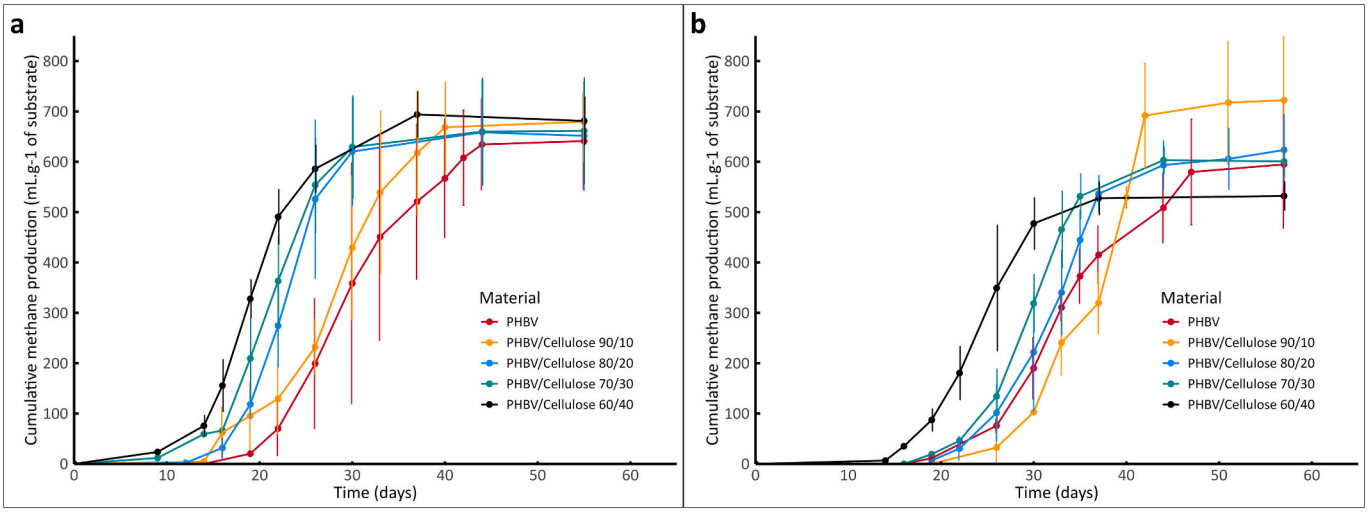

Fig. 1. Cumulative methane production (mL $CH_4{\cdot}g$ of substrate VS^{-1}) of PHBV and PHBV/Cellulose materials in 1 mm powder (a) or in 1 × 1 cm films (b).

2013; Iwańczuk et al., 2015). Iwańczuk et al. (2015) suggested that adding natural fibres into the polymer enhances its decomposition by making a structure heterogeneous and favouring the microorganisms access to biodegradable components. Conceição et al. (2023) describe that the introduction of cellulose into the PHBV matrix increases the surface roughness and brings alterations in mechanical properties, thus making the material structure more heterogeneous. These structural modifications increase the material surface area that becomes more accessible to microorganisms, thereby promoting the biodegradation process.

The effect of material surface on biodegradation was tested using 1 × 1 cm square films of PHBV or PHBV/Cellulose and the same AD conditions (Fig. 1b). As before, all materials exhibited relatively similar ultimate methane production after 40–57 days of incubation between 547 ± 24 and 750 ± 131 mL $CH_4 \cdot VS^{-1}$ (Kruskal-Wallis test with $p_{value} = 0.18$), maximal methane rate between 39 and 57 mL $CH_4 \cdot day^{-1} \cdot g\ VS^{-1}$ (Kruskal-Wallis test with $p_{value} = 0.50$), and 91 % to 103 % biodegradation (Table S3). In this form, the cellulose content in the material seems to affect the lag phase especially for the PHBV/Cellulose composite containing 40 % of cellulose. A 34 % decrease of the lag phase duration was observed between the films of PHBV/Cellulose 60/40 and of PHBV alone (Figs. 1b and S1b).

Overall, the materials in powder have a shorter lag phase than 1 × 1 cm films, ranging from 23 ± 2 to 13 ± 1 days for the materials in powder against 29 ± 3 to 18 ± 1 days for the films (differences confirmed by a paired *t*-test of lag time values between powder and films $p_{value} = 0.00295 < 0.05$). Increasing the surface area of the material (e.g. powder versus film) appears to accelerate the biodegradation process as described before and suggested in the literature (Cazaudehore et al., 2022; Uddin and Wright, 2023).

3.2. Changes in material properties during AD biodegradation

3.2.1. Monitoring of 2 × 2 cm films anaerobic biodegradation

Another set of BMP tests was performed in AD conditions at 38 °C to monitor the degradation of materials using 2 × 2 cm PHBV, PHBV/Cellulose 80/20 and 60/40 films (Fig. 2). A part of the bottles was incubated up to 63 days to measure biogas production. Another part was sacrificed every 10 days to recover film residues for material analysis and search for metabolites in the BMP liquid mediums. The methane production of the cellulose positive control reached 483 mL $CH_4 \cdot g\ VS^{-1}$ corresponding to 97 % of biodegradation at 63 days. The ultimate methane production of PHBV, PHBV/Cellulose 80/20 and 60/40 reached respectively 504 ± 107 mL $CH_4 \cdot g\ VS^{-1}$, 446 ± 109 mL $CH_4 \cdot g\ VS^{-1}$ and 526 ± 123 mL $CH_4 \cdot g\ VS^{-1}$ at the end of the experiment (Fig. 2a). No significant differences were observed between these values (Kruskal-Wallis test with $p_{value} = 0.39$), which correspond to 76 %, 78 % and 102 % biodegradation respectively.

The methane production presented two main periods across materials (Fig. 2a). The first period occurred from 0 to about 20 days, reaching a plateau of methane production of 51 mL $CH_4 \cdot g\ VS^{-1}$, 48 mL $CH_4 \cdot g\ VS^{-1}$ and 189 mL $CH_4 \cdot g\ VS^{-1}$ for respectively PHBV, PHBV/Cellulose 80/20 and PHBV/Cellulose 60/40. The second period of methane production began after 40 days for PHBV and PHBV 80/20, and 30 days for PHBV 60/40. As previously observed, the presence of 40 % of cellulose in the material significantly favoured the composite degradation.

Two-phase methane production curves have already been reported in literature for PHBV degradation in AD (Nachod et al., 2021). This phenomenon was attributed to the inhibition of methanogenesis due to the accumulation of metabolic intermediates, such as volatile fatty acids (VFA) and/or hydrogen. It usually occurs when a substrate is highly fermentable, causing bacterial hydrolysis reactions to release intermediates more rapidly than methanogenic archaea can process them. The resulting build-up of metabolic intermediates can lead to temporary or complete inhibition of methanogenesis. This effect may be increased with cellulose whose anaerobic degradation releases many different VFA, alcohols and hydrogen while PHBV degradation is expected to release butyric and valeric acids (García-Depraect et al., 2022b). Alternatively, in the case of PHBV/Cellulose composites, the two-phase methane production curves may also result from an asynchronous consumption of the composite components.

The VFA concentration in the BMP liquid mediums was measured by GC–MS along BMP tests (Fig. 2b). No volatile fatty acids were detected at the beginning and at the end of BMP incubations, with a quantification limit of 40 $ng \cdot L^{-1}$. However, acetic, butyric and isobutyric acids were identified during the anaerobic digestion process, with a maximum concentration quantified at 50 days for PHBV and 20 to 30 days for PHBV/Cellulose composites (Table S4). This suggests strong hydrolytic activities during these incubation times. Interestingly, these times also correspond to the last time when film residues could be collected in the bottles. As shown in Fig. 2c, all materials underwent a significant mass loss justafter 10 days of incubation. This mass loss reached 87 % on day 50 for PHBV films, and 47 % and 75 % for the PHBV/Cellulose 80/20 and 60/40 films on day 20, respectively. No more plastic residue was then recovered by sieving the BMP medium at 500 μm and 100 μm. This suggests that films disintegrated completely over the following 10 days. Nevertheless, biogas continued to be produced thanks to the degradation of the metabolic intermediates accumulated in the liquid medium. The persistence of small microparticles or oligomers of the materials in the BMP cannot be excluded but was not measured in this study.

A double exponential modified Gompertz growth function was used to model the two-phase methane production curves as already applied by Dragomir et al. (2021). The biodegradation levels, calculated using the Buswell equation, were around 72 % and 75 % degradation for respectively the PHBV and PHBV/Cellulose 80/20 films. The PHBV/Cellulose 60/40 appears completely degraded reaching 98 % of biodegradation within 63 days (Table S5).

3.2.2. Material surface deterioration

Scanning electron microscopy (SEM) was used to observe the alteration of the film surface during the digestion (Fig. 3).

As the biodegradation proceeds, several holes and cracks become visible on the material surfaces, more rapidly in the case of composite materials (Fig. 3). A correlation is observed between film degradation, biogas production and material mass loss. The surface of the PHBV films is only slightly altered up to 20 days (Fig. 3), corresponding to the first period of the methane production curves (Fig. 2). Then, from 30 to 40 days, many cracks appear while methane production rate reaches maximal values. After 50 days of degradation, the PHBV film surface displays craters visible at the lower magnification ×500, indicating significant decomposition. On the opposite, the PHBV/Cellulose films rapidly exhibited cellulose fibres on their surface, showing that degradation started readily during the first 10 days of incubation. Similar cracks have been observed for PHBV biodegradation at the end of BMPs (Gómez and Michel, 2013).

3.2.3. PHBV polymers deterioration

The degradation of the PHBV fraction of each material can be monitored by size-exclusion chromatography (SEC) analysis of the polymer mean molecular mass (Mw). Since this method requires the solubilisation of the material, it gives a global picture of the polymer degradation whatever its location in the material, either on surface or in the bulk. However, only the PHBV can be monitored, the cellulose being insoluble in chloroform.

The PHBV polymer molecular weight before degradation were around 140 kDa, 160 kDa and 110 kDa for respectively PHBV, PHBV/Cellulose 80/20 and PHBV/Cellulose 60/40 materials (Fig. 4). These values are lower than those reported for PHBV in literature (around 900 kDa) by Bossu et al. (2021) and Doineau et al. (2023). The polymer may have been affected by undergoing two successive extrusions and being heated through hydraulic press during materials production, which may

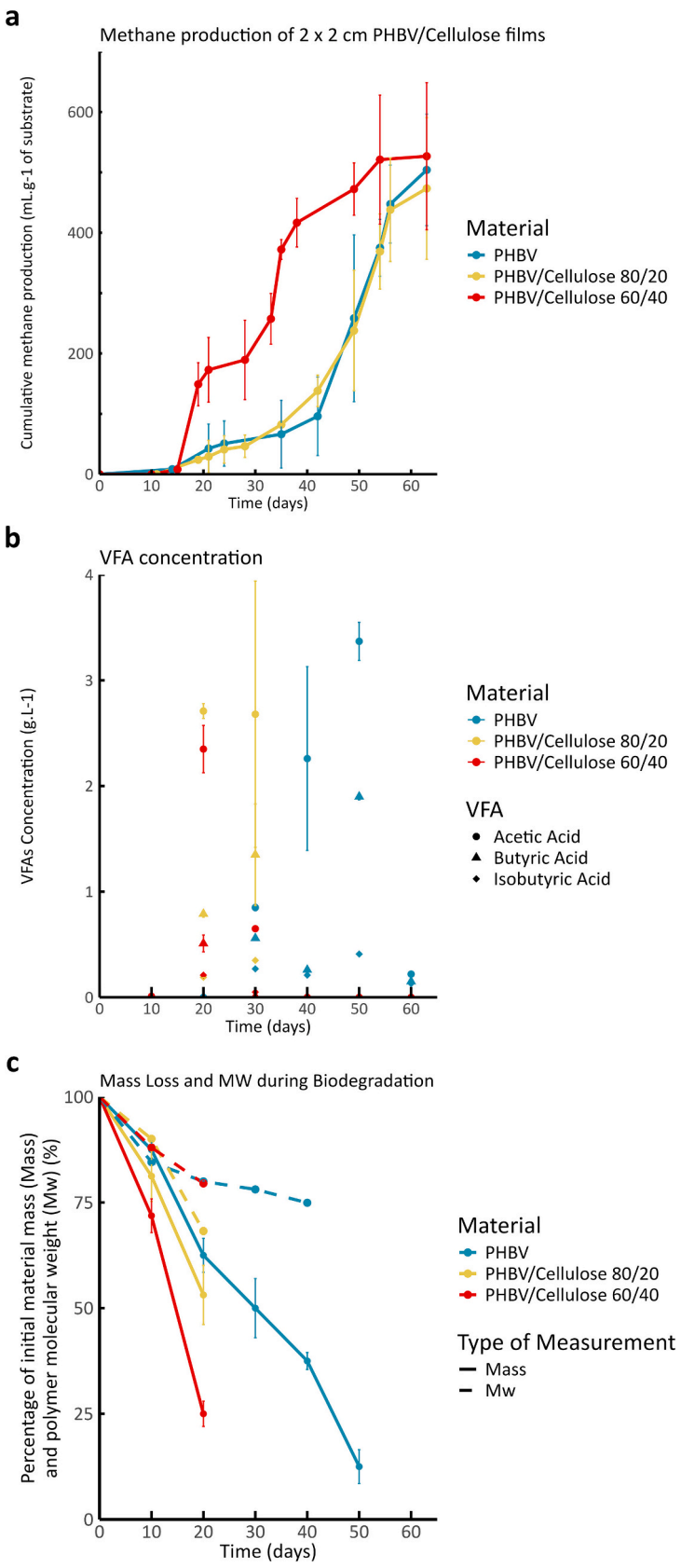

Fig. 2. Time course monitoring of PHBV and PHBV/Cellulose 2 × 2 cm films degradation during BMP tests at 38 °C for 63 days. Material conversion into methane (a) and co-metabolites (b). Mass and polymer molecular weight (Mw) of materials retrieved every 10 days, in % of the initial value (c).

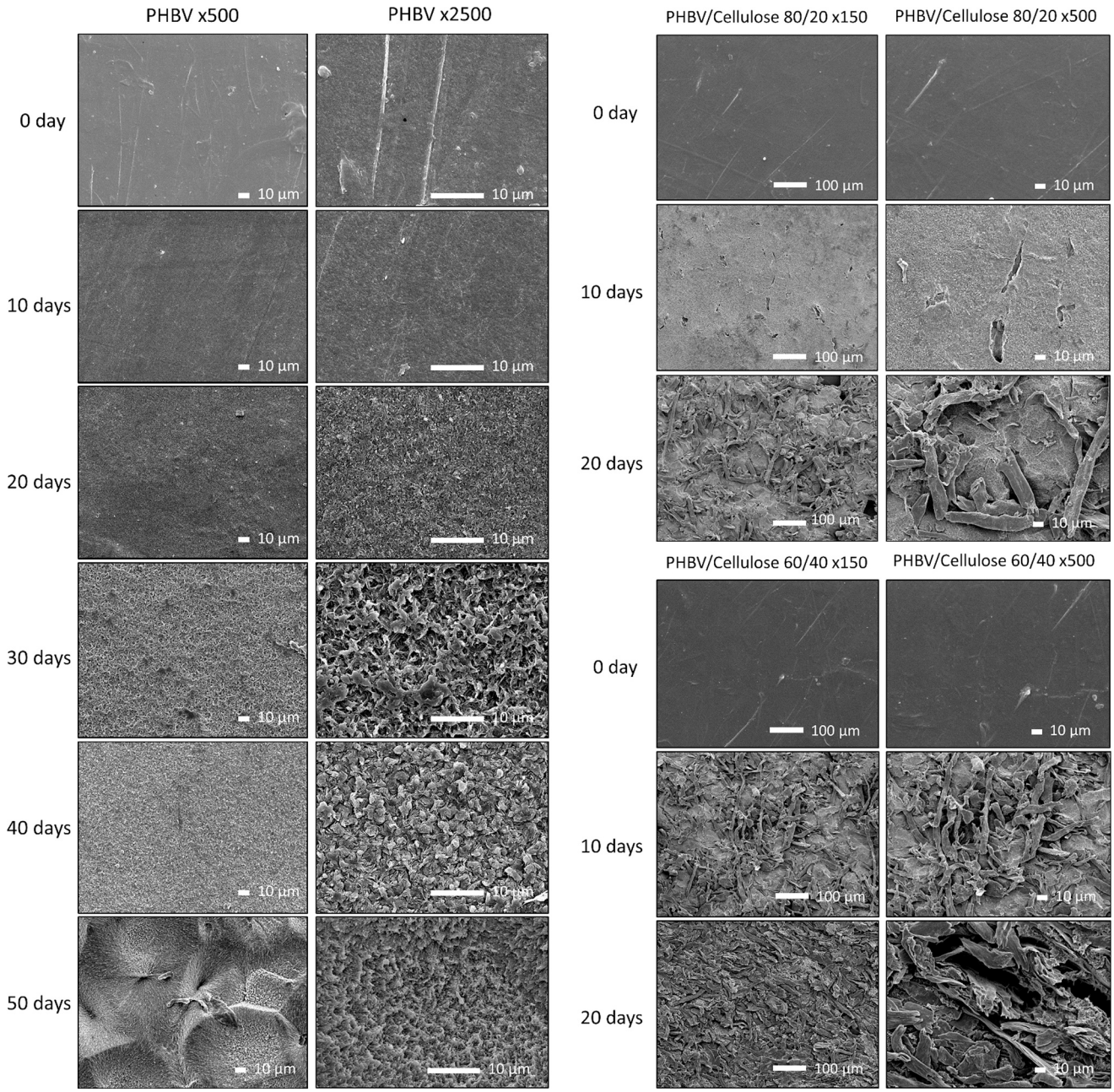

Fig. 3. SEM photographs of non-degraded (0 day) and degraded films after 10 to 50 days of anaerobic digestion at 38 °C. Two magnifications are shown for each material: 500× and 2500× for PHBV, and 150× and 500× for PHBV/Cellulose composites.

have made them more sensitive to analysis than commercial materials. Nevertheless, Fig. 4 shows a constant and almost linear reduction of the PHBV polymer Mw with time during AD. For the last materials recovered, only Mw reductions of 16 %, 31 % and 21 % were observed for respectively the PHBV, the PHBV/Cellulose 80/20 and the PHBV/Cellulose 60/40 films, meaning that the recovered materials largely retained their integrity.

As a control of abiotic degradation, a set of BMP bottles was realised with the same initial materials but in sterile water and without biological inoculum. The bottles were incubated in anaerobic conditions at 38 °C. The Mw of the PHBV polymer in the PHBV and PHBV/Cellulose 80/20 films remained quite stable for the first 20 to 30 days of AD (Fig. 4). The one of the PHBV/Cellulose 60/40 films however reduced of about 14 % after 20 days of incubation, suggesting an abiotic hydrolysis activity for this material. The same phenomenon was observed for the PHBV films after 40 days of incubation in water. Finally, for a same incubation time, the polymer Mw of all films in water was systematically higher than that of films degraded in AD conditions. This indicates that the material degradation observed in AD is mainly due to biotic factors rather than abiotic factors. Moreover, it suggests that material degradation occurs progressively from the surface of the material, probably by enzymatic hydrolysis as proposed for other biodegradable plastics (Meereboer et al., 2020b; Silva et al., 2023).

3.2.4. *Materials thermal behaviour and composition*

Thermo-gravimetric analyses (TGA) were carried out on all materials to assess their thermal behaviour as a function of their biodegradation level (Fig. S2). This analysis aims to firstly evaluate changes of material thermal stability during biodegradation, and secondly, the composition of composite materials (Ruggero et al., 2019).

For each material, its decomposition temperatures were determined as the temperatures corresponding to the maximum of the peaks

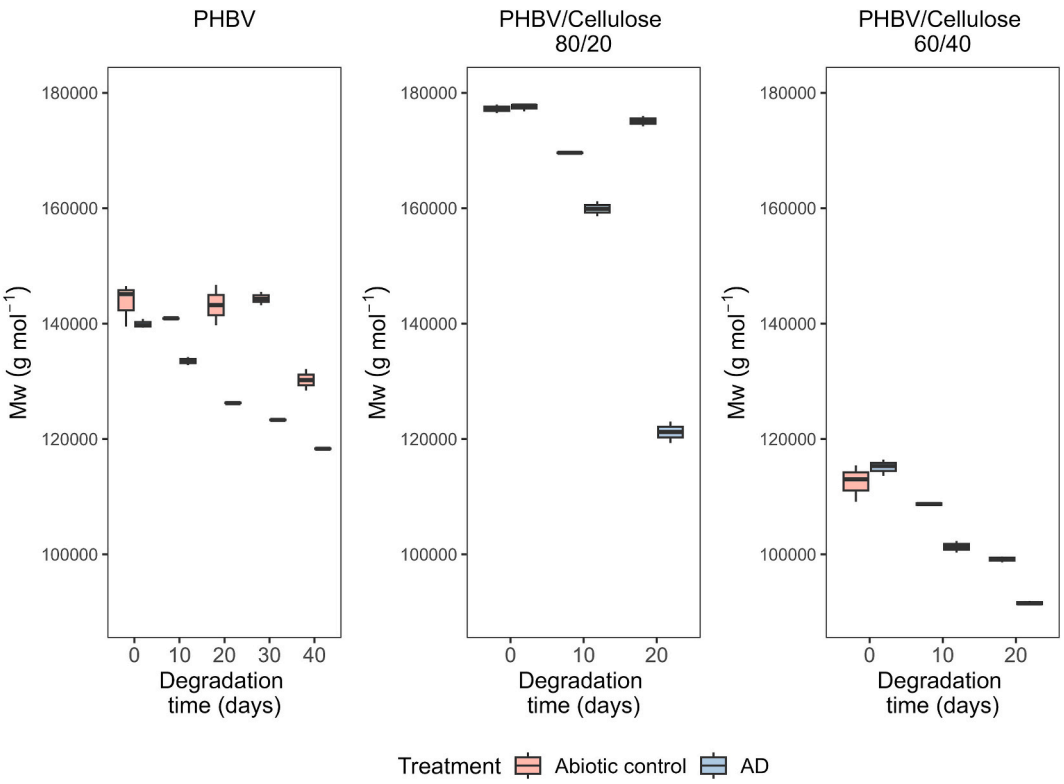

Fig. 4. Evolution of the PHBV polymer Mw in PHBV, PHBV/Cellulose 80/20 and PHBV/Cellulose 60/40 films during abiotic incubations (pink boxplots) and BMP tests (blue boxplots) at 38 °C. Letters a, b and c highlight the significant statistical differences observed with HSD tests between each material for each time in triplicate with p-value < 0.05.

obtained with the first derivative of their TGA curve. For PHBV/Cellulose composites, two maximums were obtained corresponding to the decomposition temperatures of both PHBV and cellulose (Table S6). The measured PHBV decomposition temperature was about 285 °C and the cellulose one around 345 °C, which is in accordance with values reported in literature (285 °C for PHBV and 338 °C for cellulose) (Meereboer et al., 2020b; Yeng et al., 2015). The decomposition temperatures measured for all PHBV and PHBV/Cellulose films were not significantly different before biodegradation (Kruskal test $p_{value} = 0.41 > 0.05$), and during biodegradation (Kruskal test $p_{value} = 0.39 > 0.05$ for PHBV alone; Kruskal test $p_{value} = 0.77 > 0.05$ for PHBV/Cellulose 80/20; and Kruskal test $p_{value} = 0.88 > 0.05$ for PHBV/Cellulose 60/40). This means that the percentage of cellulose in the initial PHBV composites, and the time of degradation did not strongly affect the thermal stability of material components. Although this may seem surprising, it can be explained by two hypotheses. First, the film residues recovered during the BMP tests are those that have not yet undergone severe degradation. Second, the film components that are degraded within the materials are rapidly released into the environment.

The proportion of each component within the films can be determined using the local minima of the first derivative of its TGA curve. The weight fraction of cellulose in the PHBV/Cellulose 80/20 films is similar regardless of the degradation time (Fig. S2), suggesting that both polymers are degraded or released from the film simultaneously. At the opposite, the cellulose content in the PHBV/Cellulose 60/40 films decreased from 39 % on day 10 to 24 % during the 20 days of biodegradation. This suggests that cellulose fibres are more prone to biodegradation than PHBV leading to a decrease of the cellulose content within the composite (Meereboer et al., 2020b).

3.2.5. Polymer molecular bonds cleavage

The polymers molecular bonds affected during film biodegradation were evaluated using FT-IR analysis according to Dedieu et al. (2023), Jin et al. (2022) and Xiang et al. (2016) (Table S7).

The FT-IR spectra of the PHBV and PHBV/Cellulose films do not undergo drastic changes during biodegradation before respectively day 50 and day 20 (Fig. 5 and Figs. S3 and S4). However, several differences can be pointed out. First, the spectra obtained from the most degraded materials exhibit higher values at 1020 cm^{-1}. This wavenumber is attributed to C—OH bonds due to the formation of smaller oligomers with alcohol at the end of polymer chains (Kim et al., 2023). This is in agreement with the observed reduced intensity of the 1718 cm^{-1} peak that corresponds to ester bonds, and with the changes seen at 3270 cm^{-1} wavenumber. ANOVA and Tukey's Honestly Significant Difference (HSD) tests highlight a substantial distinction among materials degraded at these wavenumbers (Figs. S5 and S6, $p_{value} < 0.05$). This emerging large band at 3270 cm^{-1} has been highlighted as resulting from the cleavage into alcohol functions of the PHBV ester bondages linking the 3-hydroxybutyric and 3-valeric acids monomers (Jin et al., 2022; Kim et al., 2023). Moreover, since this bond is broader in PHBV/Cellulose composites, and since it appears on days 20 and 10 for respectively PHBV/Cellulose 80/20 and 60/40, it could be linked to cellulose degradation. Coulon Grisa et al. (2021) showed that O—H bonds from cellulose broaden peaks around 3300 cm^{-1} in FT-IR spectra and may even affect the intensity of the C—C bonds peak at 2990 cm^{-1}. This is consistent with SEM photographs that show cellulose fibres becoming visible on the surface of PHBV/Cellulose 80/20 and 60/40 at 20 days and 10 days, respectively.

The absence of clear trend emerging from the comparison of pristine and degraded materials from days 0 to 40 days for PHBV and days 0 to 10 for PHBV/Cellulose composites suggests that there is no significant change of chemical functions on the materials retrieved during this period of degradation in AD. Since mass losses were clearly observed in Fig. 2c, it suggests that the biodegradation mainly occurs at the surface of the material and affects only the polymer's end chains, with minimal impact on the bulk material.

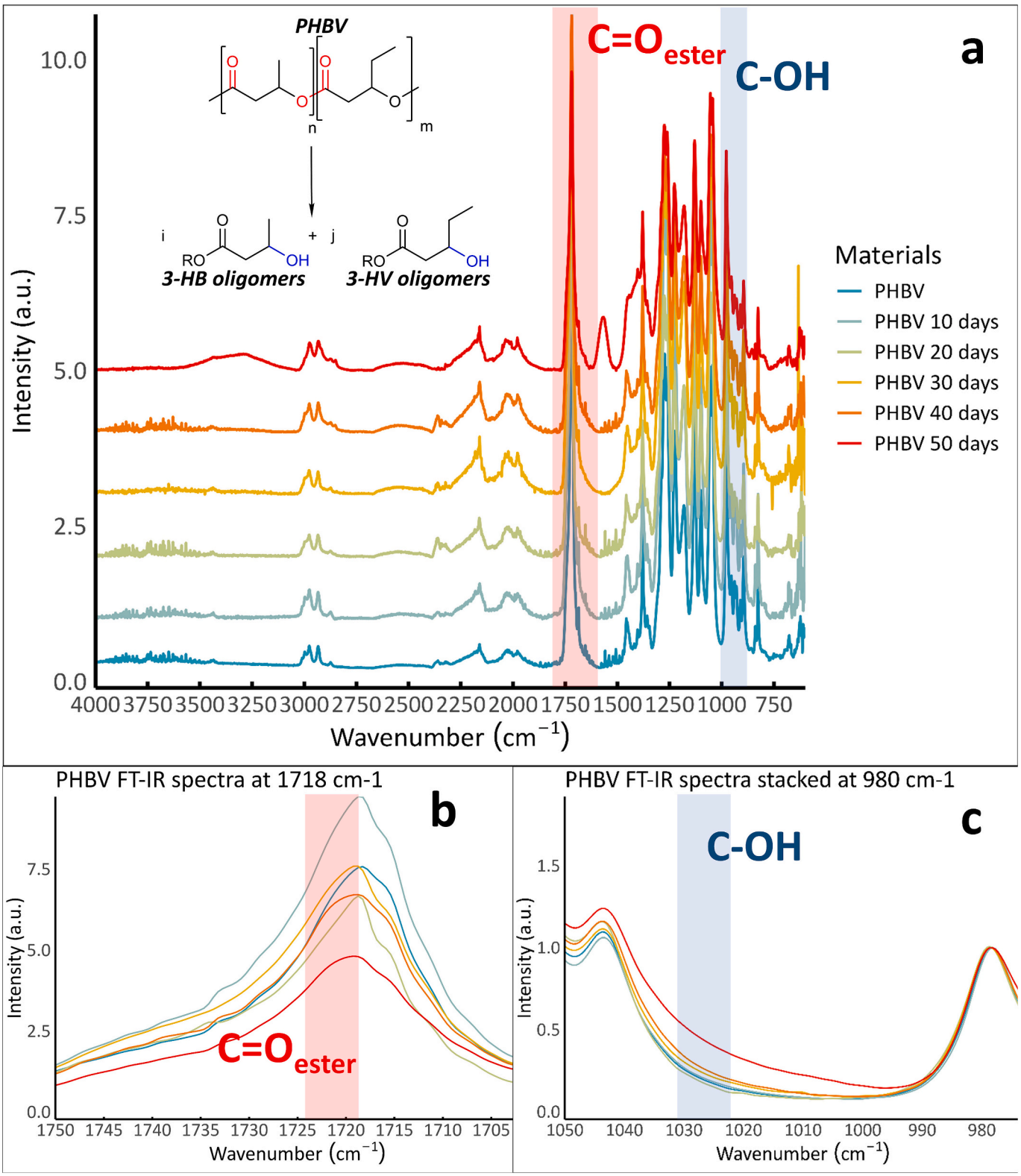

Fig. 5. Alignment of the FT-IR spectra of PHBV films at different stages of AD degradation (a). Focus on stacked spectra at 1718 cm^{-1} (C═O bond) (b) and 980 cm^{-1} (C—OH bond) (c).

The FT-IR spectra of the PHBV and PHBV/Cellulose composites incubated at 38 °C in sterile water and anaerobic conditions do not show any change between the pristine and incubated materials (Figs. S7, S8 and S9). This is in agreement with the absence of polymer cleavage observed by SEC (Fig. 4) and confirms that biotic factors predominantly explain the degradation observed during AD biodegradation.

3.2.6. *Polymer crystallinity evolution*

Crystallinity change of the materials during the AD process was studied by X-ray angle diffraction. The diffractograms indicate that all

PHBV and their cellulose composites have an orthorhombic crystalline system (Fig. S10) (Bossu et al., 2021; Chen et al., 2016). Crystallinity of the initial materials is not statistically different (Table 1, Kruskal-Wallis test with a p_{value} of 0.33 > 0.05). However, it can be noticed that as the cellulose content in the composites increases, the crystallinity percentage tends to decrease. Indeed, David et al. (2019) highlighted that incorporating fibres into the polymer matrix can reduce the available space for crystals to form during recrystallization, thereby lowering the crystallinity percentage.

During AD, the overall material crystalline percentage increases noticeably at the beginning of the biodegradation process, suggesting a degradation of the amorphous regions (Table 1). This is consistent with the literature reporting that biodegradation primarily affects the ends of polymer chain in the amorphous regions as they are less hydrophobic and more accessible to microorganisms (Shine et al., 2021). The degradation of these amorphous regions would mathematically conduct to an increase of the measured polymer crystallinity. However, another hypothesis has been proposed by Antunes et al. (2020). The cleavage of the amorphous regions of the polymer may lead to a reorganization of crystals, being consistent with the fact that these chain ends have the ability to undergo recrystallization. This later hypothesis is supported by the observation of the lattice parameters (a, b, c) and crystal size (L). As the percentage of crystallinity increases, so does the lattice parameters while the crystal size tends to decrease. It indicates that small crystals are growing during the initial phase of polymer decomposition. Additionally, the increasing width of the 020 reflection peak half intensity (WHI) during this initial degradation phase shows that the formed crystals are of lower quality than the pristine PHBV crystals (Fig. S10). This is indicative of a recrystallization process. As biodegradation progresses, crystalline regions also undergo decomposition, resulting in a decrease in the overall crystallinity index.

3.3. Microbial communities degrading the materials during AD

3.3.1. Distribution of the main phyla and genera in the planktonic and biofilm samples during biodegradation

The relative abundance of the bacterial and archaeal groups identified from the BMP liquid medium and from the biofilm attached to the PHBV and PHBV/Cellulose composites during degradation are presented in Fig. 6.

Regarding the bacteria, the *Bacillota* (formerly *Firmicutes*) appears to be the most abundant phylum identified in the planktonic communities for all materials, representing 47 ± 6 % of the total sequences. The other dominant phyla are the *Bacteroidota*, the *Proteobacteria*, and the *Spirochaetota* representing respectively 21 ± 5 %, 12 ± 7 % and 6 ± 3 % of the total bacterial sequences. These four phyla contain 86 ± 11 % of the total planktonic sequences. They include many heterotrophic microbial groups involved in the hydrolysis of complex organic matter usually found in anaerobic digestion media (Venkiteshwaran et al., 2015). The archaeal domain represents approximately 3 ± 2 % of the total sequences of the planktonic communities. *Halobacterota* is the main phylum gathering 90 ± 13 % of the total archaeal sequences with two dominant genera: the hydrogenotrophic methanogen *Methanoculleus* and the versatile methanogen *Methanosarcina* reported to be involved in the degradation of PHB along with *Candidatus Cloacimonas* (Zhang et al., 2019). The other subdominant phyla observed belong to various methanogenic *Euryarchaeota* (Falzarano et al., 2023).

The BMP planktonic community structures underwent limited fluctuations for all the tested materials over the degradation time. The most important change is a temporary increase of the relative abundance of *Thiopseudomonas* and *Clostridium* sensu stricto *7* at the beginning of the incubations, followed by the apparition of *Fibrobacterales* BBMC-4 and the methanogenic *Methanosarcina* after 40 days of incubation. *Thiopseudomonas* species are facultative anaerobes that possess many enzymatic activities such as C4 and C8 esterases (Tan et al., 2015). Members of the *Clostridium* sensu stricto genera are strict anaerobes that degrade many carbohydrates, including cellulose, to produce several VFA and alcohols like acetic, butyric and lactic acids (Wiegel et al., 2006). The *Fibrobacterales* are strict anaerobes having lignocellulosic activities that release succinic and acetic acids (Abdul Rahman et al., 2016). Finally, the hydrogenotrophic *Methanoculleus* (80 ± 21 %) is the main genus among archaea when substrates are still weakly degraded. It becomes *Methanosarcina* (78 ± 18 %) after 40 days of biodegradation for BMPs with PHBV and PHBV/Cellulose composites. *Methanosarcina* performs any of the known methanogenic pathways: acetoclastic, carboxydotrophic, hydrogenotrophic, methylotrophic, and methyl respiration (Buan et al., 2011). Its growth is favoured by high concentrations of acetate. These observations are in agreement with the rapid degradation of the complex substrates such as polymers and cellulose, that generate various metabolites after hydrolysis and acidogenesis, and the adaptation of the archaeal community that shifts from a dominant hydrogenotrophic metabolism towards a more flexible community able to produce methane by both hydrogenotrophic and acetoclastic pathways. Moreover, these observations are in line with those made in Fig. 2.

The microorganisms attached to the materials differed depending on the material (PHBV or PHBV/Cellulose films), and on the degradation time. *Bacillota* remains the main phylum present at a relative abundance between 46 ± 1 % and 81 ± 11 % of the total sequences. However, the *Clostridium* sensu stricto *7* genus becomes dominant during the degradation of PHBV films, while the degradation of PHBV/Cellulose films show the apparition of the genus *Hungateiclostridiaceae* UCG-012. Most type strains of the *Hungateiclostridiaceae* family utilize cellulose and other complex polymers as the sole carbon and energy source for growth, and produce acetate and H_2 (Zhang et al., 2019). Similarly, the early stages of PHBV/Cellulose films degradation show *Spirochaetota* becoming the second dominant phylum, mainly composed of the genus *Treponema* (22 ± 3 %), while this phylum remains low during all the degradation of PHBV films. Members of the *Treponema* genus are known to degrade lignocellulosic compounds. They have been proposed to attack the surface and hydrolyse PHBV/Cellulose composite materials at

Table 1
Crystallinity parameters measured in WAXS for PHBV and its cellulose composites. L, crystal size. a, b and c are crystal lattice parameters.

Materials	Days	Crystallinity (%)	L (nm)	WHI (°)	a	b	c
PHBV	0	74.7 ± 3	22.4 ± 0.8	0.54 ± 0.03	0.568	1.304	0.596
	10	79 ± 2	19.5 ± 0.1	0.62 ± 0.05	0.572	1.312	0.597
	20	75 ± 4	19.5 ± 0.2	0.63 ± 0.01	0.572	1.313	0.598
	30	75 ± 1	24.4 ± 0.3	0.52 ± 0.01	0.572	1.312	0.598
	40	72 ± 3.5	25.5 ± 0.3	0.49 ± 0.01	0.567	1.304	0.595
	50	70 ± 1.5	23.2 ± 0.1	0.47 ± 0.01	0.57	1.309	0.597
PHBV/Cellulose 80/20	0	72 ± 1	24.5 ± 0.1	0.47 ± 0.01	0.596	1.307	0.594
	10	75 ± 5	20.3 ± 0.6	0.54 ± 0.01	0.571	1.310	0.596
	20	73 ± 1	23.3 ± 0.1	0.50 ± 0.02	0.566	1.300	0.593
	30	71 ± 3	23.4 ± 0.1	0.48 ± 0.01	0.567	1.301	0.593
PHBV/Cellulose 60/40	0	69 ± 3	23.0 ± 0.1	0.49 ± 0.01	0.569	1.305	0.594
	10	73 ± 1	23.6 ± 0.1	0.48 ± 0.01	0.568	1.303	0.594
	20	64 ± 1	24.5 ± 0.1	0.51 ± 0.03	0.572	1.313	0.597

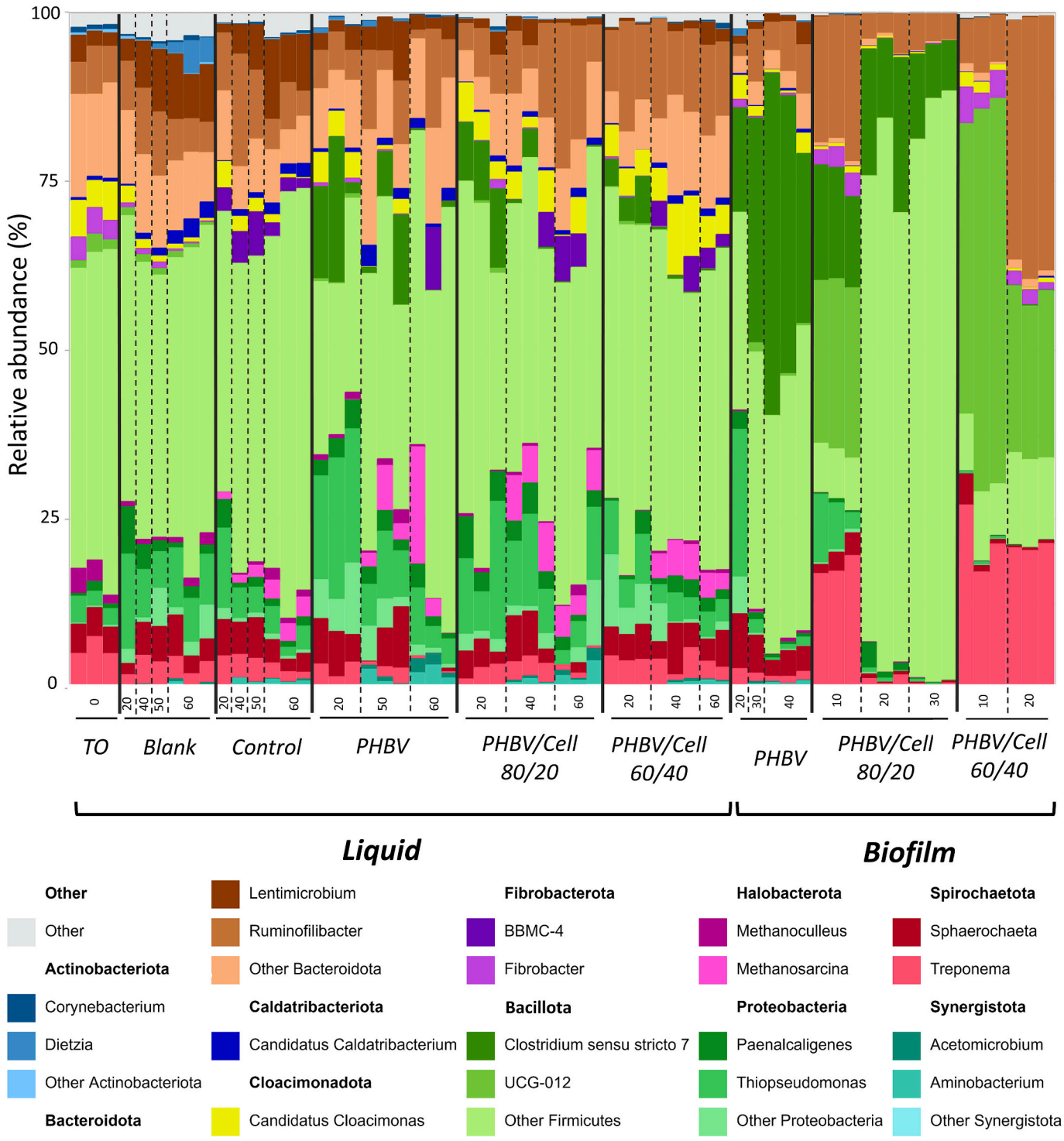

Fig. 6. Barplot representing the relative abundance of the top ten most abundant phyla and the main genera of each phylum in the BMP liquid medium and on the biofilm attached to materials. Numbers 20, 40, 50, 60 days indicate the degradation time intervals corresponding to sampling times. "Other" represent all sequences not belonging to the described phyla.

the early stage of degradation (Jensen et al., 2021; Nakasaki et al., 2020). Finally, the *Archaea* represent only 1 ± 1 % of the total sequences of the biofilm and belong mainly to the *Methanobacterium* genus at the early stage of degradation of the materials. After that, the communities move towards *Methanosphaera* and *Methanoculleus* (respectively 28 ± 26 % and 51 ± 26 % of the archaeal sequences) but remain below 0.6 % of the total sequences. All these archaeal genera are hydrogenotrophic methanogens. They may be involved in syntrophic interactions with H_2-producing bacteria such as *Hungateiclostridiaceae* UCG-012.

3.3.2. *Correlation between materials biodegradation and specific microbial clusters*

Correlations were searched between planktonic microbial communities, VFA concentrations in the BMP liquid media, and methane production. As a first step, the maximum daily methane production (rmax) on the day of sampling for microbial community characterisations was

calculated from the Gompertz modelling of the measured cumulated methane production, using the derivative of the model curve at the inflexion point (Table S8). Then a multivariate regression analysis was realised using Hellinger transformed abundance of all planktonic genera and the four environmental variables as performed by Cazaudehore et al. (2021) and Lin et al. (2016) (Fig. S11).

The three genera most correlated with rmax and the concentration of the three VFAs are *Intestinimonas*, *Gracilibacter* and *Clostridium* sensu stricto *7*. As discussed above, *Clostridium* sensu stricto 7 degrades complex polymers into many VFAs and has already been found in the biofilm of microplastics (Tang, 2023). *Intestinimonas* and *Gracilibacter* are involved in the conversion of VFAs into acetate (Hua et al., 2020; Lee et al., 2006; Crognale et al., 2023). Therefore, these genera are most probably involved in the hydrolysis, acidogenesis, and acetogenesis stages of AD, producing VFAs, such as butyric, isobutyric, and acetic acids, the latter being consumed by acetotrophic archaea.

To identify the taxa selected in biofilm, the microbial communities at the surface of plastics were compared with the planktonic communities at early stage of biodegradation in a same BMP flask on the same day using abundance differential analyses (DESEQ).

The DESEQ scatter plots show only a limited number of genera specific of the biofilm attached to the PHBV material on day 20 compared to PHBV/Cellulose composites (Fig. 7). This may be linked to its poor colonisation at this stage of the BMP, as suggested by the limited degradation of the material observed previously in Fig. 3. The highest score is for the RumEn M2 genus from the *Methanomethylophilaceae* that produces CH_4 from H_2 and formate (Table S9). The three other genera are: (i) the *Erysipelatoclostridiaceae* UCG-004 whose members of the family are known to produce isobutyrate, isovalerate and valerate; and (ii) an unidentified genus of *Pedosphaeraceae* and an *Acholeplasma*. Little information were recovered for these microorganisms except that they have saccharolytic activities producing VFA, acetate, H_2 and CO_2. None of these genera has been highlighted as potential PHBV or PHB degraders in the literature so far.

The biofilm developed on PHBV/Cellulose 80/20 highlighted several genera involved in cellulose hydrolysis in AD, i.e. *Clostridium* sensu stricto *12* and *7*, *Ruminofilibacter*, and *Ruminiclostridium*. The other genera are involved in carbohydrate fermentations and produce various VFA, alcohols, H_2 and CO_2. Finally, the PHBV/Cellulose 60/40 biofilm appeared more colonized by many hydrolytic genera such as *Hungateiclostridiaceae* UCG-012, *Fibrobacterales* BBMC4, *Treponema* and *Lutispora*. They were all reported to be linked to lignocellulolytic activities. The other observed genera are fermentative bacteria involved in the acidogenesis and acetogenesis stages of AD. The *Sporomusa* genus is doing homoacetogenesis (producing acetate from H_2 and CO_2).

According to the analyses conducted previously, possible biodegradation mechanisms of PHBV/Cellulose composites in AD along with associated main genera are gathered in Fig. 8.

4. Conclusion

To improve our understanding of biodegradable plastics degradability under anaerobic conditions, this study examined the anaerobic degradation of PHBV and of PHBV/Cellulose composites under mesophilic anaerobic conditions. PHBV exhibited very high degradation in AD regardless the dimension of materials, reaching >90 % of biodegradation in 57 days for 1 mm size powder and 1 × 1 cm films, and >60 % of biodegradation in 63 days for 2 × 2 cm films. Blending cellulose in

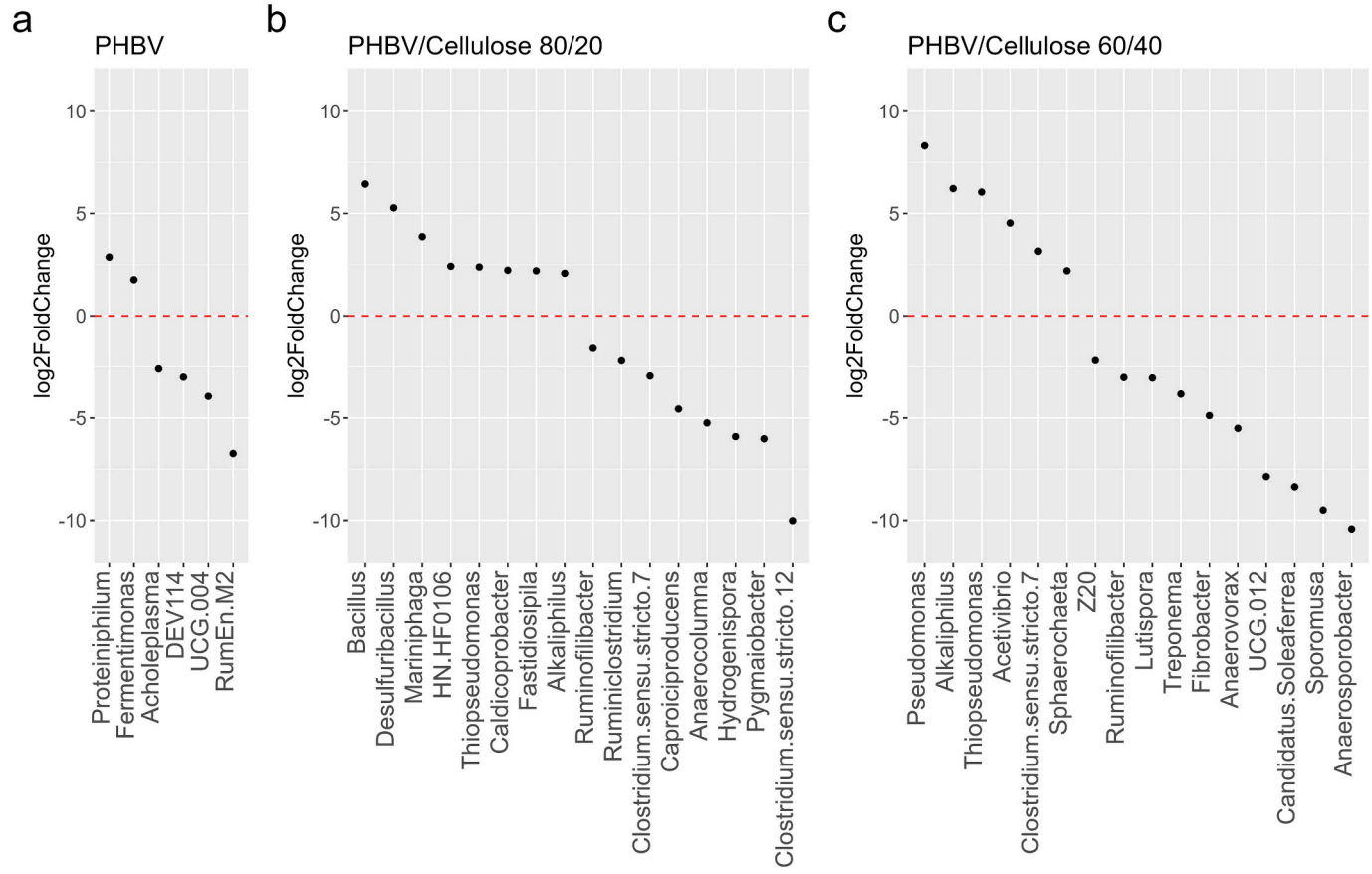

Fig. 7. Differentially abundant genera in planktonic compared to attached communities at 20 days ($p < 0.05$) for BMP with PHBV (a), PHBV/Cellulose 80/20 (b) and PHBV/Cellulose 60/40 (c). The positive log2 Fold change values correspond to genera that are significantly more abundant in the planktonic community. The negative values correspond to genera significantly more abundant in the biofilm. *f.Pedosphaeraceae* and *f.Hungateiclostridiaceae* are unidentified genera of the family level noted f.

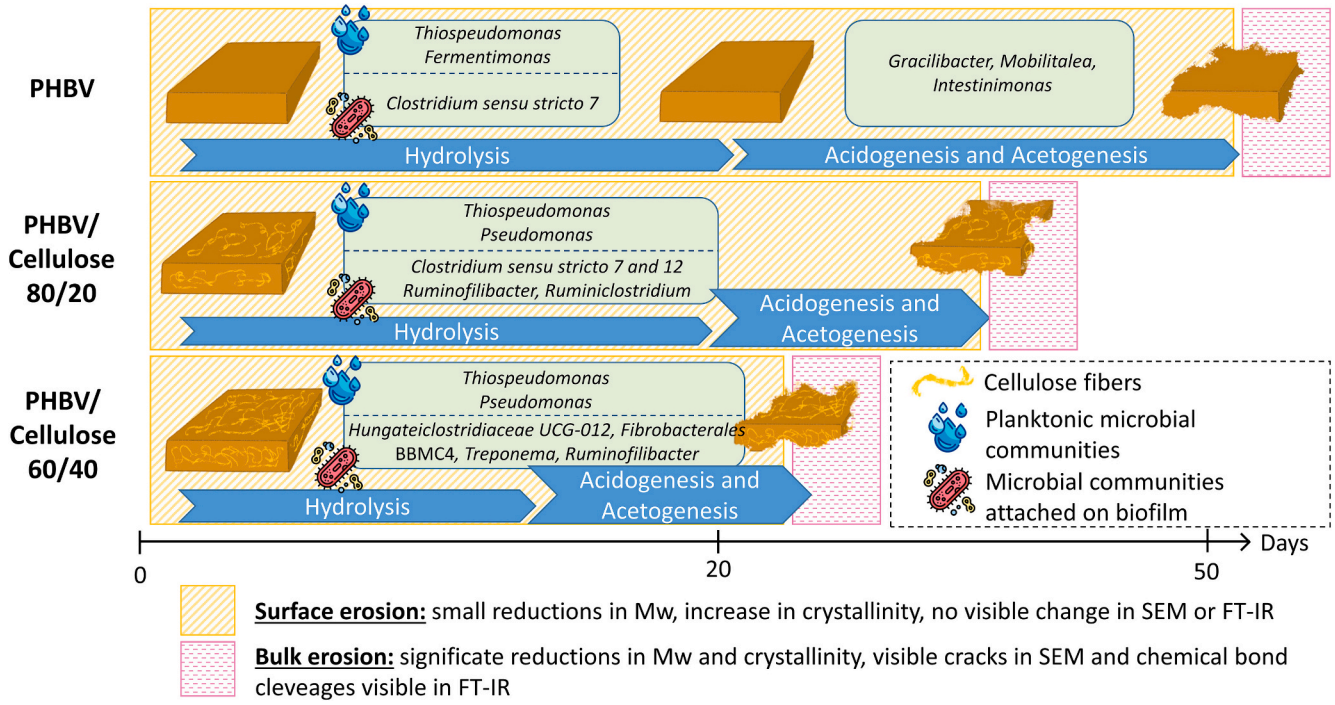

Fig. 8. The anaerobic biodegradability, possible degradation mechanisms, and functional microbes of PHBV/Cellulose composites.

polymer matrix made the degradation quicker by reducing the lag phase of methane production and accelerating films disintegration. Morphological changes and SEC, DRX and FT-IR analyses were used to follow PHBV/Cellulose material properties during biodegradation. On the onset of biodegradation, SEM photographs revealed small surface cracks and progressive mass loss, accompanied by an increase in crystallinity without alterations in FT-IR spectra. However, as degradation progressed, significant alterations in SEM and shifts in chemical bonds were evidenced by FT-IR, indicating a transition from surface erosion to bulk erosion.

Microbial communities' analysis highlighted the enrichment in specific microbial groups: *Clostridium* sensu stricto *7* appears to be involved in the hydrolysis of PHBV while *Hungateiclostridiaceae UCG 012*, *Treponema* and *Ruminofilibacter* are involved in the degradation of PHBV/Cellulose 80/20 and 60/40 within biofilm communities on material surfaces. *Thiopseudomonas*, *Fermentimonas* and *Pseudomonas* are the two main genera enriched in planktonic communities for the degradation of PHBV and PHBV/Cellulose composites.

Regarding the short degradation time of material that could match with hydraulic retention time of anaerobic digestion plants, it offers interesting prospects for PHBV and its cellulose composites disposal under anaerobic conditions.

CRediT authorship contribution statement

Paul Derkenne: Writing – original draft, Methodology, Investigation, Formal analysis, Conceptualization. **Lucile Chatellard:** Writing – review & editing, Supervision, Conceptualization. **Fabrice Béline:** Visualization, Methodology, Formal analysis. **Anne-Catherine Pierson-Wickmann:** Supervision, Resources, Methodology, Formal analysis. **Nathalie Gontard:** Supervision, Project administration, Conceptualization. **Patrick Dabert:** Writing – review & editing, Validation, Supervision, Project administration, Methodology, Funding acquisition, Conceptualization.

Funding

This work was funded by the French National Research Agency (ANR) under the ANR-21-CE43 project BioCyPlast. P. Derkenne is the recipient of an INRAE PhD fellowship supported by the metaprogram BETTER.

Declaration of competing interest

None.

Appendix A. Supplementary data

Supplementary data to this article can be found online at https://doi.org/10.1016/j.scitotenv.2024.178224.

Data availability

Data will be made available on request.

References

Abbasi, M., Pokhrel, D., Coats, E.R., Guho, N.M., McDonald, A.G., 2022. Effect of 3-hydroxyvalerate content on thermal, mechanical, and rheological properties of poly (3-hydroxybutyrate-co-3-hydroxyvalerate) biopolymers produced from fermented dairy manure. Polymers 14, 4140. https://doi.org/10.3390/polym14194140.

Abdul Rahman, N., Parks, D.H., Vanwonterghem, I., Morrison, M., Tyson, G.W., Hugenholtz, P., 2016. A phylogenomic analysis of the bacterial phylum fibrobacteres. Front. Microbiol. 6, 1469. https://doi.org/10.3389/fmicb.2015.01469.

Acharjee, S.A., Bharali, P., Gogoi, B., Sorhie, V., Walling, B., Alemtoshi, 2023. PHA-based bioplastic: a potential alternative to address microplastic pollution. Water Air Soil Pollut. 234, 21. https://doi.org/10.1007/s11270-022-06029-2.

Antunes, A., Popelka, A., Aljarod, O., Hassan, M.K., Kasak, P., Luyt, A.S., 2020. Accelerated weathering effects on poly(3-hydroxybutyrate-co-3-hydroxyvalerate) (PHBV) and PHBV/TiO_2 nanocomposites. Polymers 12, 1743. https://doi.org/10.3390/polym12081743.

Baidurah, S., 2022. Methods of analyses for biodegradable polymers: a review. Polymers 14, 4928. https://doi.org/10.3390/polym14224928.

Bher, A., Mayekar, P.C., Auras, R.A., Schvezov, C.E, 2022. Biodegradation of biodegradable polymers in mesophilic aerobic environments. Int. J. Mol. Sci. 23, 12165. https://doi.org/10.3390/ijms232012165.

Bonnenfant, C., Gontard, N., Aouf, C., 2023. PHBV-based polymers as food packaging: physical-chemical and structural stability under reuse conditions. Polymer 270, 125784. https://doi.org/10.1016/j.polymer.2023.125784.

Bossu, J., Le Moigne, N., Dieudonné-George, P., Dumazert, L., Guillard, V., Angellier-Coussy, H., 2021. Impact of the processing temperature on the crystallization behavior and mechanical properties of poly[R-3-hydroxybutyrate-co-(R-3-hydroxyvalerate)]. Polymer 229, 123987. https://doi.org/10.1016/j.polymer.2021.123987.

Buan, N., Kulkarni, G., Metcalf, W., 2011. Genetic methods for *Methanosarcina* species. In: Methods in Enzymology. Elsevier, pp. 23–42. https://doi.org/10.1016/B978-0-12-385112-3.00002-0.

Budwill, K, Fedorak, PM, Page, WJ., 1992. Methanogenic degradation of poly(3-hydroxyalkanoates). Appl. Environ. Microbiol. 58. https://doi.org/10.1128/aem.58.4.1398-1401.1992.

Cazaudehore, G., Monlau, F., Gassie, C., Lallement, A., Guyoneaud, R., 2021. Methane production and active microbial communities during anaerobic digestion of three commercial biodegradable coffee capsules under mesophilic and thermophilic conditions. Sci. Total Environ. 784, 146972. https://doi.org/10.1016/j.scitotenv.2021.146972.

Cardona, L., Mazéas, L., Chapleur, O., 2022. Deterministic processes drive the microbial assembly during the recovery of an anaerobic digester after a severe ammonia shock. Bioresour. Technol. 347, 126432. https://doi.org/10.1016/j.biortech.2021.126432.

Cazaudehore, G., Guyoneaud, R., Evon, P., Martin-Closas, L., Pelacho, A.M., Raynaud, C., Monlau, F., 2022. Can anaerobic digestion be a suitable end-of-life scenario for biodegradable plastics? A critical review of the current situation, hurdles, and challenges. Biotechnol. Adv. 56, 107916. https://doi.org/10.1016/j.biotechadv.2022.107916.

Chen, R., Zou, W., Zhang, H., Zhang, G., Qu, J., 2016. Crystallization behavior and thermal stability of poly(butylene succinate)/poly(propylene carbonate) blends prepared by novel vane extruder. In: Presented at the Proceedings of PPS-31: The 31st International Conference of the Polymer Processing Society — Conference Papers, Jeju Island, Korea, p. 050002. https://doi.org/10.1063/1.4942278.

Colombini, G., Rumpel, C., Houot, S., Biron, P., Dignac, M.F., 2022. A long-term field experiment confirms the necessity of improving biowaste sorting to decrease coarse microplastic inputs in compost amended soils. Environ. Pollut. 315, 120369. https://doi.org/10.1016/j.envpol.2022.120369.

Conceição, M.N., Santos, M.C.C.D., Mancipe, J.M.A., Pereira, P.S.C., Ribeiro, R.C.C., Thiré, R.M.S.M., Bastos, D.C., 2023. A biodegradable composite of poly (3-hydroxybutyrate-co-3-hydroxyvalerate) (PHBV) with short cellulose fiber for packaging. Mater. Res. 26, e20220615. https://doi.org/10.1590/1980-5373-mr-2022-0615.

Coulon Grisa, A.M., Colombo, T.C.A., Zattera, A.J., Nichele Brandalise, R., 2021. Thermal, mechanical and environmental degradation characteristics of polyhydroxybutyrate-co-valerate reinforced with cellulose fibers. Mater. Sci. Eng. Int. J. 5, 3–9. https://doi.org/10.15406/mseij.2021.05.00148.

Crognale, S., Massimi, A., Sbicego, M., Braguglia, C.M., Gallipoli, A., Gazzola, G., Gianico, A., Tonanzi, B., Di Pippo, F., Rossetti, S., 2023. Ecology of food waste chain-elongating microbiome. Front. Bioeng. Biotechnol. 11, 1157243. https://doi.org/10.3389/fbioe.2023.1157243.

David, G., Michel, J., Gastaldi, E., Gontard, N., Angellier-Coussy, H., 2019. How vine shoots as fillers impact the biodegradation of PHBV-based composites. Int. J. Mol. Sci. 21, 228. https://doi.org/10.3390/ijms21010228.

Dedieu, I., Aouf, C., Gaucel, S., Peyron, S., 2023. Recycled poly(hydroxybutyrate-co-valerate) as food packaging: effect of multiple melt processing on packaging performance and food contact suitability. J. Polym. Environ. 31, 1019–1028. https://doi.org/10.1007/s10924-022-02600-4.

Deroiné, M., Le Duigou, A., Corre, Y.-M., Le Gac, P.-Y., Davies, P., César, G., Bruzaud, S., 2014. Accelerated ageing and lifetime prediction of poly(3-hydroxybutyrate-co-3-hydroxyvalerate) in distilled water. Polym. Test. 39, 70–78. https://doi.org/10.1016/j.polymertesting.2014.07.018.

Doineau, E., Perdrier, C., Allayaud, F., Blanchet, E., Preziosi-belloy, L., Grousseau, E., Gontard, N., Angellier-Coussy, H., 2023. Designing poly(3-hydroxybutyrate-co-3-hydroxyvalerate) P(3HB-co-3HV) films with tailored mechanical properties. Mater. Today Commun. 36, 106848. https://doi.org/10.1016/j.mtcomm.2023.106848.

Dragomir, T.-L., Pană, A.-M., Ordodi, V., Gherman, V., Dumitrel, G.-A., Nanu, S., 2021. An empirical model for predicting biodegradation profiles of glycopolymers. Polymers 13, 1819. https://doi.org/10.3390/polym13111819.

Escudié, F., Auer, L., Bernard, M., Mariadassou, M., Cauquil, L., Vidal, K., Maman, S., Hernandez-Raquet, G., Combes, S., Pascal, G., 2018. FROGS: Find, Rapidly, OTUs with Galaxy Solution. Bioinformatics 34 (8), 1287–1294. https://doi.org/10.1093/bioinformatics/btx791.

Falzarano, M., Polettini, A., Pomi, R., Rossi, A., Zonfa, T., 2023. Anaerobic biodegradability of commercial bioplastic products: systematic bibliographic analysis and critical assessment of the latest advances. Materials 16, 2216. https://doi.org/10.3390/ma16062216.

García-Depraect, O., Lebrero, R., Rodriguez-Vega, S., Bordel, S., Santos-Beneit, F., Martínez-Mendoza, L.J., Aragão Börner, R., Börner, T., Muñoz, R., 2022a. Biodegradation of bioplastics under aerobic and anaerobic aqueous conditions: kinetics, carbon fate and particle size effect. Bioresour. Technol. 344, 126265. https://doi.org/10.1016/j.biortech.2021.126265.

García-Depraect, O., Lebrero, R., Rodriguez-Vega, S., Aragão Börner, R., Börner, T., Muñoz, R., 2022b. Production of volatile fatty acids (VFAs) from five commercial bioplastics via acidogenic fermentation. Bioresour. Technol. 360, 127655. https://doi.org/10.1016/j.biortech.2022.127655.

Geyer, R., et al., 2017. Production, use, and fate of all plastics ever made. Sci. Adv. 3, 1700782. https://doi.org/10.1126/sciadv.1700782.

Gómez, E.F., Michel, F.C., 2013. Biodegradability of conventional and bio-based plastics and natural fiber composites during composting, anaerobic digestion and long-term soil incubation. Polym. Degrad. Stab. 98, 2583–2591. https://doi.org/10.1016/j.polymdegradstab. 2013.09.018.

Habibi, S., Rabiller-Baudry, M., Lopes, F., Bellet, F., Goyeau, B., Rakib, M., Couallier, E., 2022. New insights into the structure of membrane fouling by biomolecules using comparison with isotherms and ATR-FTIR local quantification. Environ. Technol. 43, 207–224. https://doi.org/10.1080/09593330.2020.1783370.

Hua, D., Fan, Q., Zhao, Y., Xu, H., Chen, L., Li, Y., 2020. Comparison of methanogenic potential of wood vinegar with gradient loads in batch and continuous anaerobic digestion and microbial community analysis. Sci. Total Environ. 739, 139943. https://doi.org/10.1016/j.scitotenv.2020.139943.

Iwańczuk, A., Kozłowski, M., Łukaszewicz, M., Jabłoński, S., 2015. Anaerobic biodegradation of polymer composites filled with natural fibers. J. Polym. Environ. 23, 277–282. https://doi.org/10.1007/s10924-014-0690-7.

Jabeen, N., Majid, I., Nayik, G.A., 2015. Bioplastics and food packaging: a review. Cogent Food Agric. 1, 1117749. https://doi.org/10.1080/23311932.2015.1117749.

Jensen, M.B., De Jonge, N., Dolriis, M.D., Kragelund, C., Fischer, C.H., Eskesen, M.R., Noer, K., Møller, H.B., Ottosen, L.D.M., Nielsen, J.L., Kofoed, M.V.W., 2021. Cellulolytic and xylanolytic microbial communities associated with lignocellulose-rich wheat straw degradation in anaerobic digestion. Front. Microbiol. 12, 645174. https://doi.org/10.3389/fmicb.2021.645174.

Jin, Y., Cai, F., Song, C., Liu, G., Chen, C., 2022. Degradation of biodegradable plastics by anaerobic digestion: morphological, micro-structural changes and microbial community dynamics. Sci. Total Environ. 834, 155167. https://doi.org/10.1016/j.scitotenv.2022.155167.

Kedzierski, M., Cirederf-Boulant, D., Palazot, M., Yvin, M., Bruzaud, S., 2023. Continents of plastics: An estimate of the stock of microplastics in agricultural soils. Sci. Total Environ. 880, 163294. https://doi.org/10.1016/j.scitotenv.2023.163294.

Kim, J., Gupta, N.S., Bezek, L.B., Linn, J., Bejagam, K.K., Banerjee, S., Dumont, J.H., Nam, S.Y., Kang, H.W., Park, C.H., Pilania, G., Iverson, C.N., Marrone, B.L., Lee, K.-S., 2023. Biodegradation studies of polyhydroxybutyrate and polyhydroxybutyrate-co-polyhydroxyvalerate films in soil. Int. J. Mol. Sci. 24, 7638. https://doi.org/10.3390/ijms24087638.

Lebon, E., Caillet, H., Akinlabi, E., Madyira, D., Adelard, L., 2019. Kinetic study of anaerobic co-digestion, analysis and modelling. Procedia Manuf. 35, 321–326. https://doi.org/10.1016/j.promfg.2019.05.047.

Lee, Y., Cho, J., Sohn, J., Kim, C., 2023. Health effects of microplastic exposures: current issues and perspectives in South Korea. Yonsei Med. J. 64, 301. https://doi.org/10.3349/ymj.2023.0048.

Lee, Y.-J., Romanek, C.S., Mills, G.L., Davis, R.C., Whitman, W.B., Wiegel, J., 2006. *Gracilibacter thermotolerans* gen. nov., sp. nov., an anaerobic, thermotolerant bacterium from a constructed wetland receiving acid sulfate water. Int. J. Syst. Evol. Microbiol. 56, 2089–2093. https://doi.org/10.1099/ijs.0.64040-0.

Lin, Q., De Vrieze, J., Li, J., Li, X., 2016. Temperature affects microbial abundance, activity and interactions in anaerobic digestion. Bioresour. Technol. 209, 228–236. https://doi.org/10.1016/j.biortech.2016.02.132.

Lucas, N., Bienaime, C., Belloy, C., Queneudec, M., Silvestre, F., Nava-Saucedo, J.-E., 2008. Polymer biodegradation: Mechanisms and estimation techniques – A review. Chemosphere 73, 429–442. https://doi.org/10.1016/j.chemosphere.2008.06.064.

Lyshtva, P., Voronova, V., Barbir, J., Leal Filho, W., Kröger, S.D., Witt, G., Miksch, L., Saborowski, R., Gutow, L., Frank, C., Emmerstorfer-Augustin, A., Agustin-Salazar, S., Cerruti, P., Santagata, G., Stagnaro, P., D'Arrigo, C., Vignolo, M., Krång, A.-S., Strömberg, E., Lehtinen, L., Annunen, V., 2024. Degradation of a poly(3-hydroxybutyrate-co-3-hydroxyvalerate) (PHBV) compound in different environments. Heliyon 10, e24770. https://doi.org/10.1016/j.heliyon.2024.e24770.

McAdam, B., Brennan Fournet, M., McDonald, P., Mojicevic, M., 2020. Production of polyhydroxybutyrate (PHB) and factors impacting its chemical and mechanical characteristics. Polymers 12, 2908. https://doi.org/10.3390/polym12122908.

Meereboer, K.W., Misra, M., Mohanty, A.K., 2020a. Review of recent advances in the biodegradability of polyhydroxyalkanoate (PHA) bioplastics and their composites. Green Chem. 22, 5519–5558. https://doi.org/10.1039/D0GC01647K.

Meereboer, K.W., Pal, A.K., Misra, M., Mohanty, A.K., 2020b. Sustainable PHBV/cellulose acetate blends: effect of a chain extender and a plasticizer. ACS Omega 5, 14221–14231. https://doi.org/10.1021/acsomega.9b03369.

Moshood, T.D., Nawanir, G., Mahmud, F., Mohamad, F., Ahmad, M.H., Abdul Ghani, A., 2022. Sustainability of biodegradable plastics: new problem or solution to solve the global plastic pollution? Curr. Res. Green Sustain. Chem. 5, 100273. https://doi.org/10.1016/j.crgsc.2022.100273.

Nachod, B., Keller, E., Hassanein, A., Lansing, S., 2021. Assessment of petroleum-based plastic and bioplastics degradation using anaerobic digestion. Sustainability 13, 13295. https://doi.org/10.3390/su132313295.

Nakasaki, K., Nguyen, K.K., Ballesteros, F.C., Maekawa, T., Koyama, M., 2020. Characterizing the microbial community involved in anaerobic digestion of lipid-rich wastewater to produce methane gas. Anaerobe 61, 102082. https://doi.org/10.1016/j.anaerobe.2019.102082.

Porterfield, K.K., Hobson, S.A., Neher, D.A., Niles, M.T., Roy, E.D., 2023. Microplastics in composts, digestates, and food wastes: A review. J. Environ. Qual. 52 (2), 225–240. https://doi.org/10.1002/jeq2.20450.

Reischwitz, A., Stoppok, E., Buchholz, K., 1997. Anaerobic degradation of poly-3-hydroxybutyrate and poly-3-hydroxybutyrate-co-3-hydroxyvalerate. Biodegradation 8 (5), 313–319. https://doi.org/10.1023/a:1008203525476.

Ribeiro, T., Cresson, R., Pommier, S., Preys, S., André, L., Béline, F., Bouchez, T., Bougrier, C., Buffière, P., Cacho, J., et al., 2020. Measurement of Biochemical

Methane Potential of Heterogeneous Solid Substrates: Results of a Two-Phase French Inter-Laboratory Study. Water 12, 2814. https://doi.org/10.3390/w12102814.
Ruggero, F., Gori, R., Lubello, C., 2019. Methodologies to assess biodegradation of bioplastics during aerobic composting and anaerobic digestion: a review. Waste Manag. Res. 37, 959–975. https://doi.org/10.1177/0734242X19854127.
Ryan, C.A., Billington, S.L., Criddle, C.S., 2017a. Assessment of models for anaerobic biodegradation of a model bioplastic: poly(hydroxybutyrate-co-hydroxyvalerate). Bioresour. Technol. 227, 205–213. https://doi.org/10.1016/j.biortech.2016.11.119.
Ryan, C.A., Billington, S.L., Criddle, C.S., 2017b. Methodology to assess end-of-life anaerobic biodegradation kinetics and methane production potential for composite materials. Compos. Part Appl. Sci. Manuf. 95, 388–399. https://doi.org/10.1016/j.compositesa.2017.01.014.
Sánchez-Safont, E.L., Arrillaga, A., Anakabe, J., Gamez-Perez, J., Cabedo, L., 2019. PHBV/TPU/cellulose compounds for compostable injection molded parts with improved thermal and mechanical performance. J. Appl. Polym. Sci. 136, 47257. https://doi.org/10.1002/app.47257.
Shine, C.J., McHugh, P.E., Ronan, W., 2021. Impact of degradation and material crystallinity on the mechanical performance of a bioresorbable polymeric stent. J. Elast. 145, 243–264. https://doi.org/10.1007/s10659-021-09835-7.
Sholokhova, A., Ceponkus, J., Sablinskas, V., et al., 2022. Abundance and characteristics of microplastics in treated organic wastes of Kaunas and Alytus regional waste management centres, Lithuania. Environ. Sci. Pollut. Res. 29, 20665–20674. https://doi.org/10.1007/s11356-021-17378-6.
Silva, R.R.A., Marques, C.S., Arruda, T.R., Teixeira, S.C., De Oliveira, T.V., 2023. Biodegradation of polymers: stages, measurement, standards and prospects. Macromol 3, 371–399. https://doi.org/10.3390/macromol3020023.
Song, S., Lim, J.W., Lee, J.T.E., Cheong, J.C., Hoy, S.H., Hu, Q., Tan, J.K.N., Chiam, Z., Arora, S., Lum, T.Q.H., Lim, E.Y., Wang, C.-H., Tan, H.T.W., Tong, Y.W., 2021. Food-waste anaerobic digestate as a fertilizer: the agronomic properties of untreated digestate and biochar-filtered digestate residue. Waste Manag. 136, 143–152. https://doi.org/10.1016/j.wasman.2021.10.011.
Tan, W.B., Jiang, Z., Chen, C., Yuan, Y., Gao, L.F., Wang, H.F., Cheng, J., Li, W.J., Wang, A.J., 2015. Thiopseudomonas denitrificans gen. nov., sp. nov., isolated from anaerobic activated sludge. Int. J. Syst. Evol. Microbiol. 65, 225–229. https://doi.org/10.1099/ijs.0.064634-0.
Tang, K.H.D., 2023. Bioaugmentation of anaerobic wastewater treatment sludge digestion: a perspective on microplastics removal. J. Clean. Prod. 387, 135864. https://doi.org/10.1016/j.jclepro.2023.135864.
Uddin, M.M., Wright, M.M., 2023. Anaerobic digestion fundamentals, challenges, and technological advances. Phys. Sci. Rev. 8, 2819–2837. https://doi.org/10.1515/psr-2021-0068.
Venkiteshwaran, K., Bocher, B., Maki, J., Zitomer, D., 2015. Relating anaerobic digestion microbial community and process function: supplementary issue: water microbiology. Microbiol. Insights 8 (Suppl. 2), 33–44. https://doi.org/10.4137/MBI.S33593.
Vu, D.H., Mahboubi, A., Ferreira, J.A., Taherzadeh, M.J., Åkesson, D., 2022. Polyhydroxybutyrate-natural fiber reinforcement biocomposite production and their biological recyclability through anaerobic digestion. Energies 15, 8934. https://doi.org/10.3390/en15238934.
Wang, Y., Qian, P.Y., 2009. Conservative fragments in bacterial 16S rRNA genes and primer design for 16S ribosomal DNA amplicons in metagenomic studies. PLoS One 4 (10), e7401. https://doi.org/10.1371/journal.pone.0007401.
Ware, A., Power, N., 2017. Modelling methane production kinetics of complex poultry slaughterhouse wastes using sigmoidal growth functions. Renew. Energy 104, 50–59. https://doi.org/10.1016/j.renene.2016.11.045.
Wiegel, J., Tanner, R., Rainey, F.A., 2006. An introduction to the family clostridiaceae. The Prokaryotes. https://doi.org/10.1007/0-387-30744-3_20.
Xiang, H., Wen, X., Miu, X., Li, Y., Zhou, Z., Zhu, M., 2016. Thermal depolymerization mechanisms of poly(3-hydroxybutyrate-co-3-hydroxyvalerate). Prog. Nat. Sci. Mater. Inter. 26, 58–64. https://doi.org/10.1016/j.pnsc.2016.01.007.
Yeng, L.C., Wahit, M.U., Othman, N., 2015. Thermal and flexural properties of regenerated cellulose (RC)/poly(3-hydroxybutyrate) (PHB) biocomposites. J. Teknol. 75. https://doi.org/10.11113/jt.v75.5338.
Zhang, X.J., 2014. Anaerobic process. In: Comprehensive Water Quality and Purification. Elsevier, pp. 108–122. https://doi.org/10.1016/B978-0-12-382182-9.00046-3.
Zhang, L., Loh, K.-C., Zhang, J., Mao, L., Tong, Y.W., Wang, C.-H., Dai, Y., 2019. Three-stage anaerobic co-digestion of food waste and waste activated sludge: identifying bacterial and methanogenic archaeal communities and their correlations with performance parameters. Bioresour. Technol. 285, 121333. https://doi.org/10.1016/j.biortech.2019.121333.
Zhang, K., Hamidian, A.H., Tubić, A., Zhang, Y., Fang, J.K.H., Wu, C., Lam, P.K.S., 2021. Understanding plastic degradation and microplastic formation in the environment: A review. Environ. Pollut. 274, 116554. https://doi.org/10.1016/j.envpol.2021.116554.